Metallurgical and Materials Transactions B, Vol. 27B, No. 3 (June), 1996, pp. 509-525.

Transient Thermal Model of the Continuous Single-Wheel Thin-Strip Casting Process*

Guowei Li and Brian G. Thomas

Department of Mechanical and Industrial Engineering
University of Illinois at Urbana-Champaign
1206 West Green Street
Urbana, IL 61801

ABSTRACT

A transient heat transfer model (STRIP1D) has been developed to simulate the single-roll continuous strip-casting process. The model predicts temperature in the solidifying strip coupled with heat transfer in the rotating wheel, using an explicit finite difference procedure. The model has been calibrated using strip thickness data from a test caster at ARMCO Inc. and verified with a range of other available measurements. The strip/wheel interface contact resistance and heat transfer was investigated in particular, and an empirical formula to calculate this heat transfer coefficient as a function of contact time was obtained. Wheel temperature and final strip thickness are investigated as a function of casting speed, liquid steel pool depth, superheat, coatings on the wheel hot surface, strip detachment point, wheel wall thickness and wheel material.

***** This paper was prepared with the support of the U. S. Department of Energy (DOE) Award No. DE-FC07-92ID13086. However, any opinions, findings, conclusions, or recommendations expressed herein are those of the authors and do not necessarily reflect the views of DOE.

I. INTRODUCTION

Despite the simple concept proposed by Bessemer in 1846[1], the continuous casting of thin steel strip has been difficult to commercialize, in part because the process involves complex interactions between fluid flow, solidification, shrinkage and stress, which lead to serious quality problems. Six basic types of strip casting processes are currently under development world-wide[2]: (1). Single roll (melt drag); (2). Twin roll; (3). Single belt (mold-trough train); (4). Twin belt; (5). Wheel-belt; and (6). Spray deposition. Among these processes, single-roll continuous strip casting appears promising for economic production of steel sheet.

Although much effort has been made to develop the single roll strip casting process[3-6], many problems still exist. These include the formation of surface cracks, tears, folds, excessive scale[7], and internal voids or cracks. These flaws must be minimized, since hot-rolling is not available to help them. For single-roll casting of thin sections (< 1 mm), thickness variation may constitute a serious additional problem.

The thickness and quality of the strip is affected by the thermal properties of the strip, wheel cooling conditions, wheel geometry, and other process parameters. To understand how these parameters affect strip formation, mathematical models have been developed to characterize heat transfer in the process, including the prediction of the strip thickness and temperature distribution in the wheel.

Birat and coworkers (1989)[3] investigated the relation between the shell thickness and contact time experimentally for a range of continuous casting processes. They compared their shell thickness versus contact time correlation with experimental data for a tin casting process.

Several different heat conduction models of the single roll strip casting processes can be found in the literature. Papai and Mobley (1988)[8, 9] developed a two-dimensional transient finite difference model of solidifying aluminum strip on copper. They investigated the effects of non-uniform heat transfer between the strip and wheel in the width direction, and the effects of strip width-to-wheel width and cooling conditions on solidification. Contact heat transfer coefficients of 4 - 42 kW m^{-2} $°K^{-1}$ were employed, according to “poor” or “good” contact regions. Caron et al (1990)[10] simulated a twin roll casting of 2 mm bronze and aluminum strip on steel roll at casting speed 19m $min.^{-1}$ using a 1-D transient heat transfer model. The numerical model was then used to calibrate the strip/wheel interface heat transfer coefficient and the simulation results were in good agreement with their experimental data when 30 kW m^{-2} $°K^{-1}$ was chosen. Mehrotra and coworkers (1991, 1992, 1993)[11-13] developed 1-D steady heat conduction models of steel strip casting, using constant contact heat transfer coefficients of 2.5 -

15 kW m^{-2} $°K^{-1}$. Wang et al (1992)[14] applied a 1-D finite difference model to study the effects of undercooling and cooling rate on planar (splat cooling) rapid solidification of aluminum strip on copper. Contact heat transfer coefficients of 200 - 1000 kW m^{-2} $°K^{-1}$ were employed. Jacobson et al (1993)[15] used a 1-D transient finite element model to study belt casting of steel strip using a constant contact heat transfer coefficient of 1 kW m^{-2} $°K^{-1}$. Muojekwu et al (1995)[16] investigated the heat transfer and microstructure during metal solidification. In their model the interface heat transfer coefficients of 2-4 kW m^{-2} $°K^{-1}$ for contact time of 20-30 s were measured and calculated by applying a 1-D implicit finite difference model. Studies[17, 18] on single roller rapid solidification processes with short contact lengths and high casting speeds divided the interface heat transfer coefficient into high and low values for regions of good and bad contact. To match experimental data, the fitted interface heat transfer coefficient was found to decrease with increasing contact time at low casting speed. For high casting speed, a maximum heat transfer coefficient was sometimes reported. Although the contact heat transfer coefficient is known to be of critical importance to both strip quality and production rate, it has not yet been investigated in a comprehensive quantitative manner in the range important to commercial steel strip casting, based on experimental measurements.

This work aims to develop a 1-D, transient finite-difference model to simulate the entire single-wheel strip casting process, including flow and superheat dissipation in the liquid pool, solidification and cooling of the steel strip, and heat conduction in the rotating wheel. The model is then calibrated with experimental data, including measurements on a pilot strip caster by researchers at ARMCO, Inc. In particular, a time-dependent heat transfer coefficient is found to represent the contact resistance across the strip/wheel interface. The effect of important process parameters on the solidification and heat transfer are investigated using the model. Finally, a user-friendly version of the model, STRIP1D, is used at ARMCO to help further understanding and design of the process.

II. MODEL DESCRIPTION

A simplified schematic of the single roll continuous strip caster, such as that used at ARMCO, is shown in Figure 1(a). Liquid steel flows through a ceramic nozzle, forming a shallow pool against the narrow rotating copper roll or “wheel”. While in the pool, the steel solidifies against this water-cooled wheel, which rapidly withdraws the solid steel strip. After rotating along with the wheel for a certain angle, the strip is detached and air cooled on both sides.

A one-dimensional transient finite-difference model, called STRIP1D, was developed to follow temperature evolution in a slice through both the wheel and the shell, as shown in Figure 1(b). It is a Lagrangian model so there is no relative motion between either the wheel, the strip or the computational domain. The model is transient for both the strip and wheel because the wheel heats up with time. The model follows temperature development in the wheel continuously and reinitializes the steel nodes to simulate casting of a new piece of strip once every revolution.

The following assumptions greatly simplify this model:

(1) heat losses along the width direction of strip are negligible;

(2) heat conduction along the perimeter of wheel and strip is negligible:

This is justified, because the Peclet number, Pe based on a typical final strip thickness of 0.7 mm, is very large;

(3) there is no slipping between the wheel and strip;

(4) the strip thickness does not change after it gets out of the liquid pool. This assumption appears reasonable, as calculations in Appendix A show that the expected variation in thickness due to liquid drag should average about 0.1 mm. Level variation due to liquid drag is on the order of 3.5 mm.

Temperature in the strip and wheel is governed by the 1-D transient heat conduction equation in cylindrical coordinates:

$$\rho C_p^* \frac{\partial T}{\partial t} = k \frac{\partial^2 T}{\partial r^2} + k \frac{1}{r}\frac{\partial T}{\partial r} + \frac{\partial k}{\partial T}\left(\frac{\partial T}{\partial r}\right)^2 \qquad [1]$$

For the solidifying steel, the effective specific heat, C_p^*, is defined as:

$$C_p^* = \frac{dH}{dT} = C_p - \Delta H_L \frac{df_s}{dT} \qquad \text{when } T_{sol} \le T \le T_{liq} \qquad [2]$$

The solid fraction, f_s, is assumed to vary linearly between the solidus temperature T_{sol} and liquidus temperature T_{liq}, so:

$$C_p^* = C_p + \frac{\Delta H_L}{T_{liq} - T_{sol}} \qquad \text{when } T_{sol} \le T \le T_{liq} \qquad [3]$$

Both C_p and k are temperature-dependent (See Figure 2). The effect of assuming constant k or C_p (with values in Table I) is small. Details regarding the solution methodology are presented in Appendix B. Since this model is explicit, no iteration is required. There is, however,

a well-known theoretical restriction on the time step and mesh size combinations possible to achieve stable solution for this problem:

$$\frac{\Delta t \quad k}{\Delta r^2 \, \rho \, C_p^*} < 0.5 \qquad [4]$$

The time step size mainly depends on the number of cells and thermal diffusivity of the steel strip because the mesh size in the steel is much smaller than that in wheel. A fine spacing (less than 0.05 mm) is used between the nodes in the steel, requiring a small time step (less than 10^{-5} s). To accelerate the program, the time step size is increased to 10^{-3} s when the simulation domain includes only the wheel. Typically it takes 10 minutes CPU time on an IRIS4D workstation to simulate 250 seconds physical time (about 100 cycles) using this numerical model. The model has also been implemented into a user-friendly package that runs quickly on an IBM-PC computer. This program is currently being used by researchers at ARMCO to further develop the strip casting process.

The simulation domain containing the wheel and the strip is divided into five zones according to the different heat transfer conditions (see Figure 1(a) and 1(b)). They are: (I) shell growth zone, (II) strip cooling zone, (III) non-contact zone, (IV) no spray zone, (V) second non-contact zone. The strip solidifies in the pool in zone I, contacts the wheel in zones I and II, and is exposed to the environment in zones III to V. Cooling water is sprayed uniformly onto the wheel inner surface except in zone IV.

1. *Zone I (shell growth zone)*:

The simulation domain is a slice through the liquid steel, strip, interface and wheel, presented in Figure 1(b). It includes about 4 mm of solid and/or liquid steel, and about 40 mm of copper from the cold inner surface (wheel/water interface) to the outer hot surface (strip/wheel interface) of the wheel.

In this zone, the solidified shell thickness, s, is determined by linear interpolation:

$$s = (1 - f_s) * (r_{liq} - r_{si}) + f_s * (r_{sol} - r_{si}) \qquad [5]$$

Here r_{liq} and r_{sol} are the radii corresponding to T_{liq} and T_{sol} respectively, each found by linearly interpolating temperature between adjacent nodes[19]. After leaving the liquid pool, the shell thickness is fixed to the position of the closest node to the solidification front. This avoids

the complexity of adjusting the simulation mesh after each wheel revolution. In the liquid steel, the strip temperature is set initially to T_{liq}, and the temperature distribution in the solid shell is obtained by solving Equations [1] to [3] (see Appendix B for details), imposing a "superheat flux", q_{suph}, to the solid/liquid interface, as described in a later section.

Heat flux extracted by the spray cooling water at the wheel inner surface, q_{spray}, is based on an empirical formula[20] relating water flux and surface temperature, given in Appendix C.

$$q_{w1} = q_{spray} \quad [6]$$

Thermal convection boundary condition is employed at the strip/wheel interface:

$$q_{s1} = -q_{wn} = h_{gap1}(T_{s1} - T_{wn}) \quad [7]$$

The heat transfer coefficient h_{gap1} is described in detail in later section.

2. *Zone II (strip cooling zone)*:

The simulation domain for the steel is only the solid strip in this zone. Because the upper surface of the strip is exposed to the ambient air, forced convection and radiation boundary conditions are used on this surface. To match experimental measurements, it has been found that the heat transfer coefficient across the strip/wheel interface must decrease from h_{gap1} to a much lower value h_{gap2}. This reduction implies to a sharp decrease in contact between the shell and wheel, possibly related to thermal contraction induced by temperature changes in the strip.

3. *Zones III and V (non-contact zone)*:

After leaving zone II, the domain representing the solid steel strip is mathematically separated from the wheel. Both sides of the strip are exposed to air, so forced convection together with the radiation boundary conditions are applied to both upper and lower surfaces of the strip:

$$q_{s1} = (h_{air} + h_{rad,s1}) * (T_{s1} - T_{air}) \quad [8]$$

$$q_{sf} = (h_{air} + h_{rad,sf}) * (T_{sf} - T_{air}) \quad [9]$$

where, $h_{rad,s1} = \varepsilon\sigma_{SB} (T_{s1}^2 + T_{air}^2) (T_{s1} + T_{air})$; $h_{rad,sf} = \varepsilon\sigma_{SB} (T_{sf}^2 + T_{air}^2) (T_{sf} + T_{air})$.

The forced convection boundary condition is also employed on the wheel hot face:

$$q_{wn} = h_{conv} (T_{wn} - T_{air}) \quad [10]$$

The wheel/water interface boundary conditions are the same as those in the previous zones.

4. *Zone IV (no spray zone)*:

Boundary conditions for this zone are the same as those in zones III and V, except that heat transfer at the wheel/water boundary is changed to convection:

$$q_{w1} = h_{no\text{-}spray} (T_{w1} - T_{air}) \quad [11]$$

Because there is a pool of cooling water in the bottom of the rotating wheel, the heat transfer coefficient in this "no spray zone" is still much greater than that for forced convection with air, h_{conv}.

III. TREATMENT OF SOLID / LIQUID INTERFACE

A separate 3-D finite difference fluid flow and heat transfer model[21, 22] was used to calculate the heat flux profile imposed to the interface between the liquid and solidifying steel strip (shell) to account for convection of superheat in the liquid steel.

A. Fluid Model

The velocity and temperature distributions in the liquid pool were first calculated by solving the Navier-Stokes equations, k-ε turbulence model and energy balance equation using the well-known SIMPLE algorithm [ref patankar?] with upwinding on a 60x40x20 staggered mesh. The 3-D domain simulated only the liquid steel in the nozzle, and the top free surface was assumed to be flat. A comparison of 2-D and 3-D simulations proved that only a 12 mm wide strip of liquid near the side wall needed to be modeled to capture the 3-D flow pattern with uniform inlet conditions. Zero velocity was imposed at all nodes in the solid region at the bottom left of the domain, using the blocked off method. [ref patankar?] Along the internal rough solid wall at the solidification dendrite tips, the wheel velocity was imposed. Empirical "wall law" functions were applied to define the tangential velocities, K, ε and T at the near-wall grid nodes to account for the steep gradients that exist near the boundaries. Heat fluxes extracted by the nozzle bottom and side walls, were

calculated by another separate transient 3-D heat conduction model of the solid ceramic nozzle walls,[ref final report?] and applied to the corresponding boundaries of the liquid domain. A constant pouring temperature was assigned to the inlet and the moving strip surface was fixed at the liquidus temperature. Radiation was considered at the top free surface.

B. Fluid Model Results:

Typical velocity and temperature results from this model are presented in Figures 3(a), 3(b) and 3(c). Figure 3(a) shows that the hot liquid steel enters the opening weir at the bottom of the nozzle, travels toward the shell, then bends upward, and finally goes back along the top surface toward the inlet, creating a recirculation zone in the middle of the pool. This predicted flow pattern appears to match visual observations. In most of the liquid pool, except for the region very close to the wheel, the liquid steel velocity is nearly ten times smaller than the casting speed. It is interesting to notice that the flow pattern is almost two-dimensional over most of the domain. Only near the top back corner, a very weak vortex is formed.

The temperature distributions calculated within the liquid at 10 seconds after casting started and at steady state are shown in Figures 3(b) and 3(c) respectively. Temperature contours are similar and follow the flow pattern in both figures. On its way from the nozzle inlet to the rotating wheel wall, liquid steel loses very little superheat to the nozzle bottom. After it reaches the chilled wheel wall, the liquid temperature drops very quickly along the wheel and loses most of its superheat to the solidifying shell. Most of the remaining superheat is lost via radiation from the top surface. Comparing Figure 3(b) with 3(c), it is found that temperatures at steady state are higher than those at 10 seconds, since the heat lost to the nozzle bottom and side walls decreases with time. The danger of freeze-up due to this loss of superheat is small, except at startup while the ceramic nozzle is heating up.

C. Superheat Flux Boundary Condition:

The superheat flux at the solid/liquid interface was then obtained from a thermal wall law based on the resultant velocity, turbulence, and temperature fields. Figure 4 shows the superheat flux to the shell for typical conditions, (casting speed V_{c0} = 1.0 ms^{-1}; superheat temperature ΔT_0 = 75 ˚C) predicted by this turbulent fluid flow and heat transfer model of the liquid steel in the nozzle. The superheat flux delivered to the shell is relatively constant across the pool. It

increases in direct proportion to superheat temperature (the difference between the liquidus and pouring temperatures) and casting speed[21, 22]. Therefore, the superheat flux for other casting speeds and superheat temperatures can be found from q_{sh} for standard conditions at steady state by:

$$q_{suph} = \left(\frac{V_c}{V_{c0}}\right)\left(\frac{\Delta T}{\Delta T_0}\right) q_{sh} \qquad [12]$$

This superheat flux was applied to the solid/liquid interface of STRIP1D according to equations [B2] and [B3] in Appendix B. A similar method to handle superheat has been used successfully in previous work[21, 22]. It assumes that no latent heat is transported by convection through the liquid, which is consistent with perfect columnar solidification.

IV MODEL CALIBRATION OF INTERFACE HEAT TRANSFER COEFFICIENT

Heat transfer across the gap in the contact zone I is defined through the heat transfer coefficient at the strip/wheel interface h_{gap1},

$$q_{s1} = -q_{wn} = h_{gap1}(T_{s1} - T_{wn}) \qquad [7]$$

This heat transfer coefficient is the most important parameter governing heat conduction in the entire process. It depends on the micro geometry and materials of both of the surfaces of the strip and the wheel and other process conditions. Despite the many pertinent theoretical and experimental investigations[23-26], the heat transfer mechanisms across these intermittently contacting surfaces and their dependencies upon applied conditions are still not fully understood or quantified. Thus, experimental measurements were needed to calibrate the model.

Measurements were obtained from pilot strip casting trails on plain carbon steel, conducted at ARMCO[27]. A single constant value for h_{gap1} was found to be inadequate to predict shell thickness for all cases. At first, different constants were simply fit for each set of experimental conditions at ARMCO[27]. Next, a more fundamental relationship was sought.

It is postulated that the best parameter to characterize the heat transfer coefficient between the strip and wheel should be the contact time[10]. When the liquid steel first contacts the clear cold wheel surface, the heat transfer coefficient is known to have an extremely high value, and the bond is accepted to be very strong[10, 28]. As the time elapses, the solidifying shell gains in

strength and its thermal shrinkage due to the rapid cooling generates important shear stresses. These soon break the intimate bond, and a tiny gap is created between the two surfaces. The heat transfer coefficient drops accordingly with increasing time, as the shell continues to thicken and bend, further increasing the gap and lowering the heat transfer coefficient. To take this into account, the following empirical formula to calculate heat transfer coefficient between strip/wheel interface was adopted:

$$h_{gap1} = \begin{cases} h_0 & \text{when } 0 < t < t_0 \\ h_0 * \left(\frac{t_0}{t} \right)^m & \text{when } t_0 < t < t_I \end{cases} \qquad [13]$$

The three adjustable model parameters h_0, t_0 and m in Equation [13] were calibrated using numerical trial-and-error for the same series of casting experiments, according to the contact time. Figure 5 shows that the calibrated Equation [13] adequately reproduces the experimental data from ARMCO[27]. The average coefficient, found by integrating Equation [13], decreases with time as follows:

$$h_{gap1,\,avg} = \frac{1}{t_I} \int_0^{t_I} h_{gap1}\, dt = \frac{h_0\, t_0}{t_I} + \frac{h_0\, t_0}{t_I} \frac{1}{1-m} \left[\left(\frac{t_0}{t_I} \right)^{1-m} - 1 \right] \qquad [14]$$

Note that the average heat transfer coefficient $h_{gap1,\,avg}$ based on the fitted values decreases from (28 kW m^{-2} °K^{-1}) at high casting speed (1.5 ms^{-1}) to (16 kW m^{-2} °K^{-1}) at lower casting speed (0.5 ms^{-1}). This shows how the average strip/wheel interface heat transfer coefficient decreases as the contact time increases. It is also interesting to note that the fitted value for the exponent m of 0.55 is very similar to the square root time relationship expected for shell growth. This appears to demonstrate a probable link between shell deformation and heat transfer. The fitted value for t_0 of 0.01 s suggests that loss of perfect contact must occur very quickly. Also from Figure 5, it is obvious that the linear relation between the strip thickness and the contact time does not fit the experimental data.

There is also a great deal of variability in strip thickness observed in this figure. These variations were observed between local regions of the same section of strip, in addition to variations in average between different heats. They are attributed mainly to large local differences in contact heat transfer coefficient. Other factors are considered in later sections, including liquid drag (Appendix A), liquid level fluctuation and transient superheat variations. In any case, the function in Equation [13] should be considered to be an approximate spatially-averaged heat transfer coefficient.

V. MODEL VERIFICATION

To verify the model, including Equation [13] and the three calibrated constants given in Table I, the model was applied to simulate other available experimental casting data, including experiments on continuous casting, compiled by Birat et al.[4], tin strip casting[3], and "hot dip" test measurements performed at ARMCO[27, 29].

The heat flux extracted across the strip/wheel interface (while in the liquid pool) was calculated to decrease inversely with the square root of contact time, matching the Birat et al experimental cases as shown in Figure 6. In continuous strip casting, the contact time is very short, typically about 0.1 second. Thus, the heat flux to the cooling wheel, typically 10 MW m^{-2}, is much greater than that in continuous slab casting processes. The higher the casting speed, the shorter the contact time, so the average heat flux increases. Figure 7 reveals that the model using Equation [13] predicts that the strip thickness at pool exit is proportional to 0.55 power of the contact time.

The model was next used to simulate tin strip casting, and the predictions are compared with strip thickness correlation and experimental data from Birat et al[3]. To simulate the tin casting process, the casting metal properties employed in the model, such as density, specific heat, thermal conductivity, latent heat, liquidus and solidus temperatures were reset to the corresponding tin properties. Figure 8 shows that good agreement has been obtained between measured tin strip thicknesses and STRIP1D predictions. It is significant that the same heat transfer coefficient relation produces agreement with such a different casting process. The equally-good agreement between STRIP1D results and the correlation of Birat et al shows that the difference between exponents of 0.5 and 0.55 is negligible.

To further confirm the model with Equation [13], a series of "hot dip" experiments were undertaken in ARMCO Inc.[29]. In this test, a 102 x 102 x 38 mm^3 copper block, with initial uniform ambient temperature, is suddenly submerged about 10 mm deep into a liquid steel bath at 1531 ˚C as shown in Figure 9. After a short time (about 0.22 s to correspond with the strip casting process), the block is removed from the pool with a thin solidified steel strip on its bottom hot face and then cooled in ambient air. The temperatures of five thermocouples installed at different depths from the block hot face (2.95 mm, 9.30 mm, 15.65 mm, 22 mm and 28.35 mm) are recorded. Because the submerged depth is small compared with the dimensions of the copper block, the 1-D heat flow assumption inherent in STRIP1D is reasonable.

A comparison between the model predictions and measurements for a typical dip test is shown in Figure 10. The difference in quantitative matching might be due to differences of conditions between the simulation and the test and the inaccuracy of the thermocouples. During the first 0.22 seconds, all of the temperatures increase as the copper block is rapidly heated by the liquid steel. After 0.22 seconds, heat loss to ambient suddenly cools the exposed bottom surface. The solidified steel strip on the copper block insulates this heat loss somewhat. After this time, the temperatures rapidly approach the same value, the average temperature of the block, which equilibrates due to the high conductivity of the copper relative to the slow convection losses from the surfaces (i.e., low Bi number). From Figure 10, the temperature of thermocouple 1 (closest to the bottom hot face) decreases from its maximum to approach this average. The temperature of thermocouple 5 (closest to the top cold face) increases monotonically, as it is always colder than the average. The average temperature of the block gradually cools to eventually approach the ambient temperature.

It is interesting that the model with Equation [13] also appears to apply to this case with a stationary copper block and matches the measured temperatures. Based on the large range of contact time and conditions in the experimental data, and the accuracy of the model predictions, it appears that Equation [13] with the three fixed empirical constants may be universal for casting processes where liquid metal directly contacts solid metal.

VI. TYPICAL MODEL RESULTS

The mathematical model has been tested for the casting of carbon steel in the strip thickness range of 0.6 to 1.0 mm. The predicted results, including final strip thickness, strip and wheel temperature, are now presented and compared with available measurements. The results presented here were obtained by running the model under the standard casting conditions listed in Table I, except as otherwise indicated.

Figure 11 compares the predicted temperature histories of the wheel cold face and the cooling water leaving the wheel with experimental thermocouple measurements. Note that the time scale was enlarged between 150 - 152.5 s to show results during a typical revolution of the wheel. The wheel cold face temperature increases during the first 70 s approximately, to reach a quasi-steady-state condition, or a steady periodic function of time. The roughly 7 ˚C fluctuations of the wheel cold face temperature are caused by alterations of the cooling water heat transfer conditions between the spray zones and the no-spray zone. The amplitude of the variations

depends greatly on the heat flux values in the spray and no-spray zones and the period is determined by the casting speed and wheel outer radius. The wheel cold face temperature increases in the no-spray zone IV, because the heat transfer coefficient is smaller in this region.

Figure 12 shows the strip thickness at liquid pool exit as a function of casting time for standard conditions. The strip thickness increases while the liquid pool fills. Then, the thickness decreases slightly with time due to the slightly smaller heat flux associated with the hotter wheel at later times. In addition, the strip thickness is slightly larger at early times, due to the absence of superheat. After about 70 s, the strip thickness has reduced about 10%, and the conditions have reached quasi-steady state. The time to reach the quasi-steady state depends on wheel and strip properties, wheel geometry, the definition of quasi-steady state and other process parameters, but it is generally in the range of 50 to 80 seconds. Of greater importance is the larger, relatively-random fluctuation in experimental strip thickness with time and position, which is not modeled. This fluctuation is undoubtedly related to local variations in heat transfer across the interface. Thus, Eq. [13] is valid only in a time-averaged sense.

The predicted quasi-steady state temperatures of the hot and cold surfaces of the wheel are given in Figure 13. The hot surface temperature increases in zone I. This is because the heat flow from the wheel cold surface to the cooling water is much less than that from the strip to the wheel hot surface in zone I. After zone I, the hot face temperature decreases continuously, due to thermal equilibration in the wheel. This figure also illustrates the function for h_{gap1}, which decreases rapidly with contact time in zone I.

The typical temperature distribution in the strip at quasi-steady state with standard conditions is presented in Figure 14. It is found that the temperatures of both sides of the strip decrease very fast as soon as the strip leaves the liquid pool of zone I. Further loss of contact between the strip and wheel is believed to cause a further drop in interfacial heat transfer between zones I and II (see Figure 13). This causes the inner surface of the strip to quickly reheat to equal the outer temperature, which could generate detrimental thermal stresses. Temperature within the strip soon becomes almost uniform across its thickness, because the strip is so thin.

To demonstrate that the numerical model works properly, heat balances in the strip and wheel can be calculated at any desired time. For standard conditions, (see Table II), the heat balance on the strip while in the liquid pool indicates that most of the heat extracted to the wheel comes from latent heat of solidification (69%), with cooling of the strip accounting for 24% and superheat extraction only 10%. Heat enters the wheel mainly in zone I (76%), due to contact with the hot strip, and 25% more in zone II. Heat losses from the wheel exterior due to convection and

radiation cooling in zone III-V are negligible (less than 1% of the total heat lost). Heat loss to the cooling water is almost uniformly distributed per unit length around the wheel interior perimeter, and almost equals the total heat extracted from the strip for these quasi-steady state conditions. Numerical errors for the heat balance are always less than 5%.

VII. EFFECT OF CASTING CONDITIONS

The casting speed, liquid steel pool depth, coatings on the wheel hot surface, superheat, strip detachment point and wheel wall thickness and material all affect the casting process. To understand and compare the effects of these casting parameters, a set of cases were studied whose conditions are given in Table III.

A. *Effect of Casting Speed:*

The speed of the rotating wheel, or casting speed is, perhaps, the most important parameter that affects the operation of the caster. Figure 15 shows how strip thickness varies with casting speed. To cast thicker strip requires longer residence time of the solidifying strip in the liquid steel pool. One way to achieve this is by lowering the casting speed. As shown in Figure 15 and discussed previously, the numerical prediction of the final strip thickness matches the experimental data used to calibrate the model. The results are also consistent with previous observations that the average strip/wheel interface heat transfer coefficient increases monotonically with increasing casting speed due to the shorter contact time[17, 18].

The temperatures predicted on the wheel hot face and cold face are given in Figure 16 for "sliding thermocouples" which are fixed in space at the initial pool/wheel junction. The wheel hot face temperature increases with casting speed, while the wheel cold face temperature is much less sensitive. This is attributed to the small contact time, and large average heat transfer coefficient across the strip/wheel interfacial gap in the high casting speed case. The consequence is a higher temperature gradient in the wheel at higher casting speed, which would likely be detrimental to wheel life.

B. *Effect of Liquid Steel Pool Depth:*

The contact time of the solidifying strip with the liquid steel in zone I increases in direct proportion with both the contact angle, θ_1, and contact length L_1. This length is determined by the liquid pool depth, d_{pool}, wheel outer radius, R_o, and the angular position θ_0 of the liquid pool in zone I.

$$L_1 = \frac{2\pi R_o \theta_1}{360} = \frac{2\pi R_o \left[\sin^{-1} \left(\frac{d_{pool}}{R_o} + \sin \theta_0 \right) - \theta_0 \right]}{360} \qquad [15]$$

Thus, the final strip thickness increases with increasing pool depth, as shown in Figure 17. The effects of pool depth and casting speed together control the shell thickness, via the contact time, t_I:

$$s\ (mm) = 2.0\ t_I^{0.55}(s) \qquad [16]$$

where

$$t_I = \frac{L_1}{V_c} \qquad [17]$$

The non-linear increase of strip thickness with contact time is almost exactly matched by the non-linear increase of the pool depth with contact time (length). Thus, for the range of conditions simulated in this work (40 mm < d_{pool} < 120 mm), the final strip thickness is almost directly proportional to the pool depth.

Variations in pool depth produce changes in strip thickness. A variation in pool depth of 10 mm (16%) produces a strip thickness variation of about 0.07 mm (10%) (see Figure 17). In conclusion, the liquid level should be controlled to keep the strip thickness uniform.

C. *Effect of Coatings on Wheel Hot Face:*

Coating the wheel outer surface with a thin plate of Ni or Cr has a significant effect on the wheel temperature. Figure 18 presents the comparison of the quasi-steady state wheel temperatures on the cold and hot surfaces for the case with a 2 mm Ni coating layer (Case 7) versus standard conditions (Case 1). Property data for the coating materials were taken from the handbook[30]. The total wheel thicknesses in these two cases are the same. Owing to the smaller

conductivity and specific heat of the coating materials, these layers act as heat insulators, to decrease the average heat flux to the copper wheel. This lowers the wheel surface temperature outside zone I, and lowers the copper temperature everywhere. The temperature in the Ni layer is much higher than that in the corresponding copper layer with no coating in zone I due to the small conductivity of Ni. This is predicted to decrease the final strip thickness, but the effect is extremely small. The same conclusions can be obtained from the results of the other cases with coatings in Table IV. It should be noted that changing wheel material and temperature might influence the heat transfer across the strip/wheel gap, which was ignored here.

D. *Effect of Superheat :*

Superheat contained in the liquid steel acts to slow down solidification of the shell because it must be removed first. A comparison between the final strip thicknesses for zero superheat and 68 ˚C superheat is presented in Figure 19. Even for this large increase in superheat, the final strip thickness is predicted to decrease by only about 0.04 mm. This shows that superheat has very little effect on the strip thickness.

To account for the initial absorption of superheat from the liquid by the cold refractories, the superheat flux was initially set to zero. It was gradually increased to steady-state using the following empirical relation, which is based on calculations of transient heat-up of the refractories.[ref final report?]

$$q_{suph}(t) = q_{suph} \exp\left(-\frac{25}{t}\right) \qquad [18]$$

Figure 12 compares the effect of this transient equation for increasing superheat with both experimental measurements and standard results, which assume steady superheat flux. Figure 12 shows that this transient effect is very small relative to the observed variations in shell thickness.

E. *Effect of Strip Detachment Point:*

The strip is totally detached from the wheel between zones II and III. The effect of this strip detachment point on the strip thickness and temperature distribution in wheel is almost negligible. Increasing the zone II contact distance by 100 mm (25%), caused the wheel surface temperature to increase only 3%. This increase in detachment point had little effect on other

parameters such as final strip thickness, which decreased less than 0.01 mm (less than 1%). This is because the most dramatic drop in heat transfer coefficient occurs much earlier (moving from zone I to II) due to loss of contact on the micro-scale.

F. *Effect of Wheel Wall Thickness:*

The wheel wall thickness is an important design parameter of the caster. Firstly, it determines the thermal resistance to heat flow from the strip to the spray water. Naturally, the wheel surface temperature increases in almost direct proportion to wheel thickness. However, the rate of heat withdrawal does not change much with wall thickness, so the final strip thicknesses for different wheel wall thicknesses are almost the same (only 1.5% difference). The effect of wheel surface temperature change with time on the water-side heat transfer coefficient is taken into account in the empirical Equation [13]. Secondly, the time needed to reach quasi-steady-state temperature also increases with the wheel thickness. Finally, the hotter, thicker wheel is more likely to produce thermal distortion, which could interfere with the wheel roundness and good uniform sealing between the wheel and the nozzle. Poor sealing can initiate "freeze-up", where liquid enters the gaps and adheres to the nozzle instead of the wheel, quickly stopping casting.

G. *Effect of Wheel Wall Material:*

The wheel thermal properties (thermal conductivity, specific heat and density) have a big effect on the wheel temperature (the steel wheel temperature is about 220% higher than copper wheel temperature). A comparison between a steel wheel and a copper wheel with the same geometry was made, and the results are presented in Table IV. A steel wheel has a much higher hot face temperature due to the poor thermal conduction of steel. This lowers the heat transfer rate, and produces 30% thinner strip, for a given set of casting conditions. It also delays the time needed to reach quasi-steady state.

VIII. CONCLUSIONS

In the present study, a simple but realistic mathematical model of strip solidification coupled with wheel heat transfer has been developed to describe the single-roll strip casting process. The simulation results have been calibrated with available measurements, and good agreement has been obtained between calculations and a wide range of experimental data.

The model has been implemented into a user friendly program for the IBM-PC and is serving as an active research tool. In addition, conclusions predicted by this model include:

1. Heat transfer in the strip casting process is controlled mainly by the heat transfer coefficient between the solidifying strip and copper wheel. On average, this coefficient decreases with contact time, according to a function that appears valid over a wide range of casting processes. $h = (28 \frac{kW}{m^2 °K}) (\frac{0.01}{t(s)})^{0.55}$ for $t > 0.01$ s.

2. Contact time is the most influential parameter on the final strip thickness. Longer contact times produce thicker strip with approximately the same exponential dependency of 0.55 that governs the interfacial heat transfer coefficient.

3. Shell thickness increases in almost direct proportion with pool depth and is inversely proportional to casting speed. This follows from the dependency of contact time on pool depth and casting speed.

4. Coatings on the wheel hot surface have a significant effect on wheel temperature in the liquid pool zone, but negligible effect on shell thickness.

5. Transient heat up of the wheel takes 50 to 70 seconds. This may have a significant influence on pilot-plant experiments with short run times. There is even a slight influence on strip thickness.

6. A thinner wheel reaches quasi-steady state faster than a thicker wheel.

7. Superheat has only a small effect on the final strip thickness and wheel temperature.

ACKNOWLEDGMENTS

The authors wish to thank R. Williams, J. R. Sauer, R. C. Sussman of ARMCO Inc., (Middletown, OH) for providing experimental data and testing of the STRIP1D program. The steel company ARMCO Inc., Department of Energy and National Science Foundation (Grant No. MSS-8957195) are gratefully acknowledged for funding which made this research possible.

APPENDIX A. CALCULATION OF THE LIQUID STEEL LAYER DRAGGED OUT OF POOL

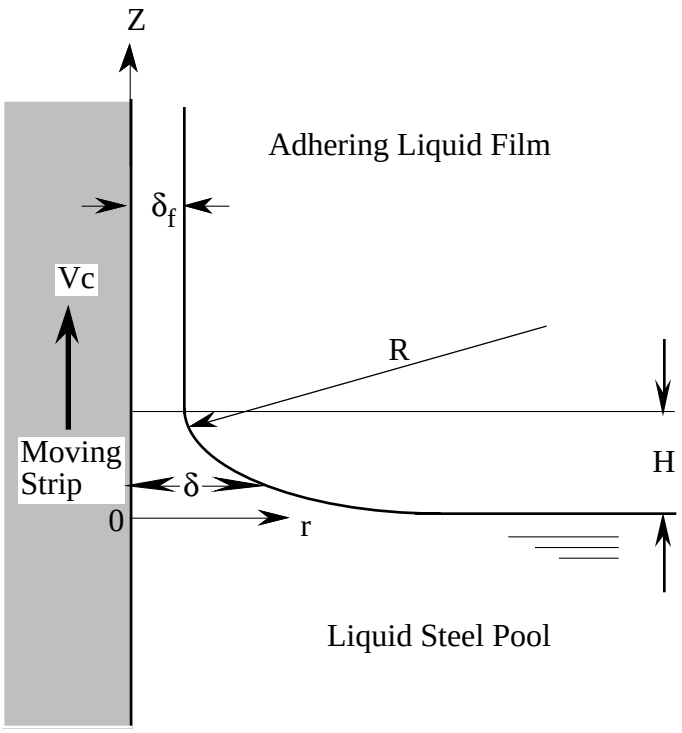

Figure A1. Close-up Schematic of Top Corner of Figure 1(a)

A liquid steel layer adheres to the moving solidified strip and is dragged out of the liquid pool[3]. The thickness and shape of the free surface depend on a force balance between the viscous forces, surface tension, inertia and gravity. The viscous forces and speed of the moving strip tend to drag the liquid upward, and inertia, surface tension and gravity tend to oppose this motion. Scaling estimation calculations show that viscous force is the largest of these forces and gravity the smallest. The magnitude of the inertia is mainly depends on the speed of the moving strip, which produces a Reynolds number of :

$$\mathrm{Re} = \frac{\rho V_c R}{\mu} = \frac{7400 \text{ x } 1 \text{ x } 0.0035}{3.85 \text{ x } 0.001} = 6700. \qquad [A1]$$

Due to the difficulty of including the non-linear inertia term, the height and thickness of this liquid steel layer has been estimated using Prostein's solution[31], ignoring the inertia and the gravity terms.

The effect of the slope of the moving strip is small. The Marangoni effect (forces induced by the surface tension variations due to the high temperature gradients) is also small, so can be neglected[32].

With these assumptions, the steady state momentum balance equation in the direction of the moving strip becomes:

$$0 = -\frac{dp}{dz} + \mu \frac{d^2V_z}{dr^2} \qquad [A2]$$

with boundary conditions:

non-slip velocity at wall: $V_z = V_c$ at $r = 0$ [A3]

zero shear stress at free surface: $\frac{dV_z}{dr} = 0$ at $r = \delta$ [A4]

Pressure is related to surface tension through curvature of the free surface:

$$p = p_0 - \frac{\sigma}{R} = p_0 - \frac{\sigma \frac{d^2\delta}{dz^2}}{[1+ (\frac{d\delta}{dz})^2]^{3/2}} \cong p_0 - \sigma \frac{d^2\delta}{dz^2} \qquad [A5]$$

Differentiating [A5] and substituting into [A2]:

$$\sigma \frac{d^3\delta}{dz^3} + \mu \frac{d^2V_z}{dr^2} = 0 \qquad [A6]$$

An analytical solution to equations [A3], [A4] and [A6] was found by Prostein[31].

$$\delta_f = 1.34\ Nca^{2/3}\ R \qquad [A7]$$

where capillary number Nca and radius of curvature R are:

$$Nca = \frac{\mu V_c}{\sigma} = \frac{0.00385 \text{ x } 1.}{1.788} \cong 0.003 \qquad [A8]$$

$$R = \sqrt{\frac{\sigma}{2\rho g}} = \sqrt{\frac{1.788}{2 \text{ x } 7400 \text{ x } 9.8}} \cong 3.5 \text{ mm} \qquad [A9]$$

Substituting equation [A8] and [A9] into [A7], the thickness of the liquid steel dragged out of the pool is estimated to be:

$\delta_f \cong 0.1$ (mm)

The maximum height of the liquid steel dragged out of the pool, H, should be less than the radius of curvature of the meniscus, estimated to be about 3.5 mm. It should be pointed out that instabilities due to transverse surface tension forces would likely make the thickness and height of this liquid steel layer more variable. Numerical simulation is needed to obtain a more accurate solution[33, 34]. However, for this pool geometry, the value of 3.5 mm appears in rough agreement with visual observations of the level fluctuations of the turbulent free surface.

APPENDIX B. SOLUTION METHODOLOGY

Equation [1] is solved at each time step using a 1-D finite difference discretization. The simulation domain, a slice through the liquid steel, solid shell, interface and wheel, was presented in Figure 1(b).

The specific heat is treated as a function of temperature in strip and wheel, the conductivity is assumed to be linear to the temperature in steel and a constant in wheel. Using the central difference scheme, the following equations are derived from Eq. [1] to [3].

A. *Liquid Steel Nodes*: (si > sf)

$$T_{si} = T_{liq} \qquad (t < t_I) \qquad [B1]$$

B. *Solid/liquid Interface Node:*

$$T_{sf}^{new} = T_{sf} + \frac{2\,\Delta t\, k}{\Delta r^2\, \rho\, C_p^*}\,(T_{sf-1} - T_{sf}) + \frac{\Delta t}{\rho\, C_p^*}\,\frac{\partial k}{\partial T}\,\left(\frac{q_{sf}}{k}\right)^2$$

$$+ \frac{\Delta t\, q_{sf}}{\rho\, C_p}\,\left(\frac{1}{r_{sf}} + \frac{2}{\Delta r}\right) \qquad [B2]$$

$$\text{where } q_{sf} = \begin{cases} q_{suph} = \left(\frac{V_c}{V_{c0}}\right)\left(\frac{\Delta T}{\Delta T_0}\right) q_{sh} & (t < t_I) \\ -q_{air} = -h_{air}^* (T_{sf} - T_{air}) & (t_I < t < t_{II}) \end{cases} \qquad [B3]$$

To ensure latent heat is not missed, a post-iterative correction is performed after each time step. Whenever a solidifying node cools below the solidus, or a liquid node cools below the liquidus, its temperature is adjusted to account for any incorrect change in enthalpy that occurred during that time step[19].

C. *Interior Strip Nodes:* ($1 \le si < sf$)

$$T_{si}^{new} = T_{si} + \frac{\Delta t \;\; k}{\Delta r^2 \, \rho \, C_p^*} (T_{si-1} - 2\, T_{si} + T_{si+1}) + \frac{\Delta t \;\; k}{2\, r_{si}\, \Delta r \, \rho \, C_p^*} (T_{si+1} - T_{si-1})$$

$$+ \frac{\Delta t}{4\, \Delta r^2 \;\; \rho \, C_p^*} \frac{\partial k}{\partial T} (T_{si+1} - T_{si-1})^2 \qquad (t < t_{II}) \qquad [B4]$$

D. *Strip Cold Face Node:*

$$T_{s1}^{new} = T_{s1} + \frac{2\, \Delta t \;\; k}{\Delta r^2 \, \rho \, C_p^*} (T_{s2} - T_{s1}) - \frac{\Delta t \, q_{s1}}{\rho \, C_p^*} \left(\frac{1}{r_{s1}} + \frac{2}{\Delta r} \right)$$

$$+ \frac{\Delta t}{\rho \, C_p^*} \frac{\partial k}{\partial T} \left(\frac{q_{s1}}{k} \right)^2 \qquad [B5]$$

$$\text{where: } q_{s1} = \begin{cases} h_{gap1} * (T_{s1} - T_{wn}) & (h_{gap1} \text{ see Eq.[13]}) \quad (t < t_I) \\ (h_{air} + h_{rad,s1}) * (T_{s1} - T_{air}) & (t_I < t < t_{II}) \end{cases} \qquad [B6]$$

The model can deal with up to four different materials in the wheel. For example, equations are presented here for a wheel of two different materials A and B, representing a copper wheel with a coating. The interface node between A and B corresponds to node number wc. For nodes in wheel material A (wi < wc, and wi is node index for wheel), constant properties k_{wA}, ρ_{wA}, C_{pwA}, α_{wA} and cell spacing Δr_{wA} are used. For nodes in wheel material B (wi > wc), properties k_{wB}, ρ_{wB} , C_{pwB}, α_{wB} and cell spacing Δr_{wB} are used.

E. *Wheel Hot Surface Node:*

$$T_{wn}^{new} = T_{wn} + \frac{2\, \Delta t \;\; k_w}{\Delta r_w^2 \, \rho_w \, C_{pw}} (T_{wn-1} - T_{wn}) - \frac{\Delta t \, q_{wn}}{\rho_w \, C_{pw}} \left(\frac{1}{r_{wn}} + \frac{2}{\Delta r_w} \right) \qquad [B7]$$

$$\text{where: } q_{wn} = \begin{cases} -q_{s1} = -h_{gap1} * (T_{s1} - T_{wn}) & (t < t_I) \\ -q_{s1} = -h_{gap2} * (T_{s1} - T_{wn}) & (t_I < t < t_{II}) \\ h_{conv} (T_{wn} - T_{air}) & (t > t_{II}) \end{cases} \qquad [B8]$$

F. *Interior Wheel Nodes:*

$$T_{wi}^{new} = T_{wi} + \frac{\Delta t \ \ k_w}{\Delta r_w^2 \, \rho_w \, C_{pw}} (T_{wi-1} - 2\,T_{wi} + T_{wi+1})$$

$$+ \frac{\Delta t \ \ k_w}{2\, r_{wi} \, \Delta r_w \, \rho_w \, C_{pw}} (T_{wi+1} - T_{wi-1}) \qquad [B9]$$

G. *Interface Node Between Different Wheel Materials:*

Substitute wn by wc in Eq. [B7] with q_{wc} satisfying:

$$q_{wc} = \frac{\frac{\alpha_{wB}}{(\Delta r_{wB})^2} * (T_{wc+1} - T_{wc}) - \frac{\alpha_{wA}}{(\Delta r_{wA})^2} * (T_{wc-1} - T_{wc})}{\frac{\alpha_{wB}}{\Delta r_{wB}\, k_{wB}} + \frac{\alpha_{wA}}{\Delta r_{wA}\, k_{wA}} + \frac{\alpha_{wB}}{2 r_{wc}\, k_{wB}} + \frac{\alpha_{wA}}{2 r_{wc}\, k_{wA}}} \qquad [B10]$$

H. *Wheel Cold Surface Node:*

$$T_{w1}^{new} = T_{w1} + \frac{2\,\Delta t\, k_w}{\Delta r_w^2 \, \rho_w \, C_{pw}} (T_{w2} - T_{w1}) - \frac{\Delta t \, q_{w1}}{r_{w1} \, \rho_w \, C_{pw}} \left(\frac{1}{r_{w1}} + \frac{2}{\Delta r_w}\right) \qquad [B11]$$

$$\text{where } q_{w1} = \begin{cases} q_{spray} \quad \text{see Eq. [C1] and [C2]} & \text{in zone I-III and V} \\ h_{no\text{-}spray} * (T_{w1} - T_{water}) & \text{in zone IV} \end{cases} \qquad [B12]$$

To ensure latent heat is not missed, a post-iterative correction is performed after each time step. Whenever a solidifying node cools below the solidus, or a liquid node cools below the liquidus, its temperature is adjusted to account for any incorrect change in enthalpy that occurred during that time step[19].

APPENDIX C. HEAT FLUX AT SPRAY WATER/WHEEL INTERFACE

Heat flux extracted by the spray cooling water at the wheel inner surface is based on the following empirical formula[20] relating water flux and surface temperature:

$$q_{spray} = B * \exp(A) \qquad [C1]$$

$$A = 12.83 - 1.40 \times 10^{-10} V_w^2 + 2.13 \times 10^{-6} * V_w * T + 0.015 * T - 3.92 \times 10^{-5} * T^2$$

$$+ 2.66 \times 10^{-8} * T^3 - 2.42 \times 10^{-15} * V_w * T^4 \qquad [C2]$$

The empirical constant A, given by Chen[20], is originally for Ni alloy with spray loading of 300 l m^{-2} $min.^{-1}$ to 1500 l m^{-2} $min.^{-1}$, surface temperature of 150°C to 850 °C. To account for the effect of different materials, constant B was introduced according to Jeschar et al[35] (B = 1.8 for copper). This formula was then linearly interpolated between the heat flux at 150 °C and 0 at 30 °C to determine values for the wheel inner surface temperature in this work.

Table I. Standard Simulation Conditions and Nomenclature

Symbol	Variable	Value	Unit
C_p	strip specific heat (steel) (see Figure 2)	690	J kg^{-1} °K^{-1}
C_{pw}	wheel specific heat (copper)	866	J kg^{-1} °K^{-1}
C_{pwater}	water specific heat	4179	J kg^{-1} °K^{-1}
C_p*	effective specific heat	see Eq. [3]	J kg^{-1} °K^{-1}
d_{pool}	pool depth	64	mm
f_s	solid fraction at solid/liquid interface	0.7	
h	heat transfer coefficient		
h_{air}	forced convection coefficient	50	W m^{-2} °K^{-1}
h_0	empirical constant in h_{gap1} , see Eq. [13]	28	kW m^{-2} °K^{-1}
h_{gap1}	strip/wheel interface heat transfer coefficient in zone I (see Eq. [13])		
h_{gap2}	strip/wheel interface heat transfer coefficient in zone II	200	W m^{-2} °K^{-1}
$h_{no\text{-}spray}$	wheel/water heat transfer coefficient in zone IV	12,000	W m^{-2} °K^{-1}
H	height of the liquid layer dragged out of the liquid pool (see Figure A1)		mm
ΔH_L	strip latent heat fusion of steel	271.96	kJ kg^{-1}
k	strip conductivity (steel) (see Figure 2)	29	W m^{-1} °K^{-1}
k_w	wheel conductivity (copper)	380.16	W m^{-1} °K^{-1}
L_1 - L_5	length along wheel outer perimeter of zones I -- V	80, 372, 585, 479, 399	mm mm
m	empirical exponent in h_{gap1} , see Eq. [13]	0.55	
Pe	Peclet number = $\frac{V_c\, s}{\alpha}$		
q	heat flux		Wm^{-2}
q_{spray}	heat flux extracted by spray water in zone I,II,III,V		Wm^{-2}
q_{sh}	superheat flux added at shell/liquid interface of standard case in fluid flow model		Wm^{-2}
q_{suph}	superheat flux added at shell/liquid interface		Wm^{-2}

r	distance from wheel center		m
r_{liq}	distance from wheel center at the position where the corresponding temperature is T_{liq}		
r_{sol}	distance from wheel center at the position where the corresponding temperature is T_{sol}		
Δr	cell spacing		m
R	radius of the meniscus curvature (see Figure A1)		mm
R_i	wheel inner radius	0.2667	m
R_o	wheel outer radius	0.3048	m
Re	Reynolds number		
s	final strip thickness		mm
t	time from start of casting		sec
t_0	empirical reference time in h_{gap1} see Eq. [13]	0.01	sec
t_I	contact time in zone I		
t_{II}	contact time in zone II		
Δt	time increment		
T	temperature		˚K
T_{air}	ambient temperature	30	˚C
T_{init}	wheel initial temperature	50	˚C
T_{liq}	steel liquidus temperature	1530 (2786)	˚C (˚F)
T_{pour}	pour temperature	1600 (2919)	˚C (˚F)
T_{sol}	steel solidus temperature	1520 (2768)	˚C (˚F)
T_{water0}	initial water temperature into spray zone	50	˚C
ΔT	superheat temperature		˚K
ΔT_0	superheat temperature of standard condition in the fluid flow model	75	˚K
V_c	casting speed	0.766 (150)	ms^{-1} ($ft\ min.^{-1}$)
V_{c0}	casting speed of standard condition in fluid flow model	1.0 (197)	ms^{-1} ($ft\ min.^{-1}$)
w	total flowrate of spray water	0.00615 (98)	$m^3\ s^{-1}$ (GPM)
W	width of strip	0.3048 (12)	m (inch)
α	thermal diffusivity of strip = $\frac{k}{\rho C_p}$		

α_c	thermal diffusivity of coating = $\frac{k_c}{\rho_c C_{pc}}$		
α_w	thermal diffusivity of wheel = $\frac{k_w}{\rho_w C_{pw}}$		
δ	liquid layer thickness dragged out of the pool (see Figure A1)		mm
δ_f	final δ far from liquid pool (see Figure A1)		mm
ε	strip emissivity (steel)	0.8	
ε_w	wheel emissivity (copper)	0.5	
μ	viscosity of the liquid steel	3.85×10^{-3}	Pa s
ρ	strip density (steel)	7400	kg m^{-3}
ρ_w	wheel density (copper)	8950	kg m^{-3}
ρ_{water}	water density	995	kg m^{-3}
σ_{SB}	Stefan-Boltzmann constant	5.678×10^{-8}	W m^{-2} $°K^{-4}$
σ	surface tension of free surface in liquid pool	1.788	N m^{-1}
θ_0	angle at start of zone I (see Figure 1(a))	30°	
$\theta_1 - \theta_5$	subtented angles of zones I to V	15°, 70°, 110°, 90°, 75°	

Subscripts:

(see Figure 1(b))

s	pertaining to strip
w	pertaining to wheel
1, i, n	node numbers (Figure 1(b) and Appendix B) (increasing from small to large radius)
f	pertaining to solidification front

Table II Heat Balance at Steady State (Standard Conditions)

A. Heat balance on strip		**(kW)**	**(%)**
1. Region I:	Heat input to shell inside (superheat):	123	10
	Latent heat:	826	69
	Sensible heat from cooling strip:	292	24
	Numerical error	-45	-3.7
	Heat loss from strip to wheel:	1196	100
2. Region II:	Heat loss from strip to ambient:	118	25
	Heat loss from shell to wheel:	387	82
	Numerical error	-31	-6.6
	Sensible heat from cooling strip:	474	100
B. Heat balance on wheel			
	Heat into wheel from strip or ambient in zone I	1196	76
	Heat into wheel from strip or ambient in zone II	387	25
	Heat into wheel from strip or ambient:	-10	-0.6
	Numerical error	-1	-0.06
	Heat loss to water	1572	100

Table III Simulation Conditions

Cases	Casting speed (ms^{-1})	Liquid steel pool depth (˚)	Coatings (mm)	Strip detachment point (˚)	Wheel wall thickness (mm)
1 standard	0.766	15.1	no	85	38
2	1.5	15.1	no	85	38
3	1.0	15.1	no	85	38
4	0.5	15.1	no	85	38
5 pool depth	0.766	20.05	no	85	38
6 pool depth	0.766	30.0	no	85	38
7 coating	0.766	15.1	2mm Ni	85	36+2
8 coating	0.766	15.1	10mm Ni 10mm Cr	85	38+20
9 detachment point	0.766	15.1	no	105	38
10 wheel thickness	0.766	15.1	no	85	20
11 steel wheel	0.766	15.1	no	85	38

Table IV. Simulation Results at Steady State

Cases	Final strip thickness (mm)	Water ΔT(°C)	Temperature on wheel inner and outer surface (°C)			
			Inner Surface		Outer Surface	
			Max	Min	Max	Min
1 Standard	0.66	18	95	89	249	162
2	0.47	23	103	98	277	196
3	0.60	20	96	92	259	174
4	0.95	14	84	80	222	132
5	0.78	20	98	92	260	173
6	0.97	23	105	98	277	191
7	0.61	17	91	87	385	156
8	0.59	16	86	83	533	294
9	0.65	19	95	90	256	168
10	0.67	18	94	88	210	119
11	0.46	12	80	75	805	624

REFERENCES

1. Bessemer, H., *U. S. Patent* , Report No. 49053, 1865.

2. Brimacombe, J.K. and Samarasekera, I.V.: "Fundamental Aspects of the Continuous Casting of Near-Net-Shape Steel Products", *Proc. International Symposium on Casting of Near Net Shape Products*, Sahai, Y.,Battles, J.E.,Carbonara, R.S.and Mobley, C.E., eds., ISS, Hawaii, 1988, pp. 3-11.

3. Birat, J.P., Blin, P., Jacquot, J.L., Riboud, P. and Thomas, B.: "Near Net Shape Continuous Casting of Flat Products at IRSID", *Revue Met.*, 1989, vol. 86, pp. 920-930.

4. Birat, J., Larrecq, M., Lamant, J. and Petegnief, J.: "The Continuous Casting Mold: A Basic Tool for Surface Quality and Strand Produtivity", in *Mold Operation for Quality and Productivity*, , Iron and Steel Society, Warrendale, PA, 1991, pp. 3-14.

5. Kumar, A. and Mehrotra, S.P.: "A Mathematical Model of Single Roll Strip Caster Based on Macroscopic Enthalpy Balances", *Steel Research*, 1991, vol. 62, pp. 164-170.

6. Sousa, A.C.M., Liu, X. and Lenard, J.G.: "Modelling of Single-Roll Continuous Strip Casting", *Proc. of the 9th International Heat Transfer Conference*, Jerusalem, Israel, 1990, pp. 419-424.

7. Grubb, J.F., Love, D.B., Murthy, A. and Nauman, J.D.: "Casting Specialty Steel Strip", in *Near Net Shape Casting*, ISS, Warrendale, 1987, pp. 51-57.

8. Papai, J.P. and Mobley, C.E.: "A Two Dimensional Time-Dependent Thermal Model for the Solidification of Sheet on Moving Substrates", *Proc. International Symposium on Casting of Near Net Shape Products*, Sahai, Y.,Battles, J.E.,Carbonara, R.S.andMobley, C.E., eds., ISS, Honolulu, Hawaii, 1988, pp. 51-62.

9. Papai, J.P. and Mobley, C.E.: "The Effect of nonuniform contact on the Solidification of Aluminum Sheet on Copper Substrates", *Proc. International Symposium on Casting of Near Net Shape Products*, Sahai, Y.,Battles, J.E.,Carbonara, R.S.andMobley, C.E., eds., ISS, Honolulu, Hawaii, 1988, pp. 79-90.

10. Caron, S., Essadiqi, E., Hamel, F.G. and Masounave, J.: "Numerical Modelling of Heat Transfer in High Productivity Rate Twin-Roll Casting Process", *Proc. Light Metals*, Bickert, C.M., eds., The Minerals, Metals & Materials Society, 1990, pp. 967-973.

11. Mallik, R.K. and Mehrotra, S.P.: "Mathematical Modelling of Single Roll Continuous Steel Strip Caster on Fluid Flow and Heat Transfer Considerations", *ISIJ*, 1993, Vol. 33, pp. 595-604.

12. Kumar, M.K.A. and Mehrotra, S.P.: "Mathematical Model of Single Roll Strip Caster Based on Microscopic Heat Balance", *Ironmaking and Steelmaking*, 1992, vol. Vol. 19, No. 1, pp. 55-63.

13. Mehrotra, S.P. and Tandon, R.: "A Mathematical Model of Single Roll Continuous Strip Caster Based on Fluid Mechanics Considerations", *Steel Research*, 1992, vol. 63 (No. 5), pp. 205-211.

14. Wang, G.-X. and Matthys, E.F.: "Numerical Modelling of Phase Change and Heat Transfer during Rapid Solidification Processes: Use of Control Volume Integrals with Element Subdivision", *Int. J. Heat Mass Transfer,* 1992, vol. 35 (1), pp. 141-153.

15. Jacobson, N., Hollinger, B. and Fredriksson, H.: "On the Development of a Thin Strip Caster", *Scand. J. Metallurgy,* 1993, vol. 22, pp. 75-82.

16. Muojekwu, C.A., Samarasekera, I.V. and Brimacombe, J.K.: "Heat Transfer and Microstructure During the Early Stages of Metal Solidification", *Metall. Trans.*, 1995, vol. 26 (April), pp. 361-382.

17. Takeshita, K. and Shingu, P.H.: "Thermal Contact during the Cooling by the Single Roller Chill Block Casting", *Transactions of the Japan Institute of Metals,* 1986, vol. 27 (6), pp. 454-462.

18. Granasy, L.: "Analysis of the Ribbon Formation Process on the Single Roller Rapid Solidification Technique", *Transactions of the Japan Institute of Metals,* 1986, vol. 27 (1), pp. 51-60.

19. Thomas, B.G. and Ho., B.: "Spread Sheet Model for Continuous Casting", *Proc. Materials Processing in Computer Age,* TMS-AIME, New Orleans, LA, 1991, vol. , pp. 293-306.

20. Chen, J., Zhu, J.Q., Rogall, C.-M. and Kopp, R.: "Untersuchungen zur Warmeubertragung bei der Spritzwasserkuhlung", *Steel Research,* 1989, vol. 60, pp. 550-560.

21. Li, G. and Thomas, B.G., "Freeze-up Prediction for Single-Roll Strip Casting", *University of Illinois at Urbana-Champaign report (Report to ARMCO Inc.),* August 10, 1992.

22. Huang, X., Thomas, B.G. and Najjar, F.M.: "Modeling Superheat Removal during Continuous Casting of Steel Slabs", *Metall. Trans.*, 1992, vol. 23B, pp. 339-356.

23. Fletcher, L.S.: "Recent Developments in Contact Conductance Heat Transfer", *Journal of Heat Transfer,* 1988, vol. 110, pp. 1059-1070.

24. Snaith, B., Probert, S.D. and O'Callaghan, P.W.: "Thermal Resistances of Pressed Contacts", *Applied Energy,* 1986, vol. 22, pp. 31-84.

25. Snaith, B., O'Callaghan, P.W. and Probert, S.D.: "Use of Interstitial Materials for Thermal Contact Conductance Control", *AIAA Paper,* 1984, No. 84-0145.

26. Robertson, S.R. and Fascetta, E.F.: "An Analytical Technique for the Determination of the Thermal Contact Resistance between a Solidifying Metal and Mold", *Metallurgical Transactions B,* 1977, vol. 8B (December), pp. 619-624.

27. Williams, R., Single-wheel Strip Casting Experiments, *private communication,* ARMCO Inc., Middletown, OH, 1992.

28. Maringer, R.M.: *The Role of Surface in Continuous Casting*. Casting of Near Net Shape Product. 1988, 351-362.

29. Williams, R., Hot Dip Experiments, *private communication*, ARMCO Inc., Middletown, OH, 1993.

30. Avallone, E.A. and III, T.B.: *Marks' Standard Handbook for Mechanical Engineers*, McGRAW-HILL book Company, 1978.

31. Probstein, R.F.: *Physicochemical Hydrodynamics*, John Wiley & Sons, Inc., 1994.

32. Gutierrez, E.M. and Szekely, J.: "A Mathematical Model of the Planar Flow Melt Spinning Process", *Metallurgical Transactions B*, 1986, vol. 17B, pp. 695-703.

33. Gutierrez, E.M.: "A Mathematical Model of the Strip Casting Process", *Proc. Casting of Near Net Shape Products*, Sahai, Y.,Battles, J.E.,Carbonara, R.S.andMobley, C.E., eds., ISS, 1988, pp. 31-38.

34. Zhang, H. and Moallemi, M.K.: "Numerical Simulation of Hot-Dip Metallic Coating Process", *Int. J. Heat Mass Transfer*, 1995, vol. 38 (2), pp. 241-257.

35. Jeschar, R., Reiners, U. and Scholz, R.: "Heat Transfer during Water and Water-Air Spray Cooling in the Secondary Cooling Zone of Continuous casting Plants", *Proc. Steelmaking Proceedings of Fifth International Iron and Steel Congress*, Iron and Steel Society, Washington, 1986, vol. 69, pp. 511-521.

LIST OF FIGURES

(a) Velocity Field (b) Superheat Temperature Field (10s) (c) Superheat Heat Temeprature Field (Steady State)

Figure 3 Velocity and Superheat Temperature in the Liquid Pool

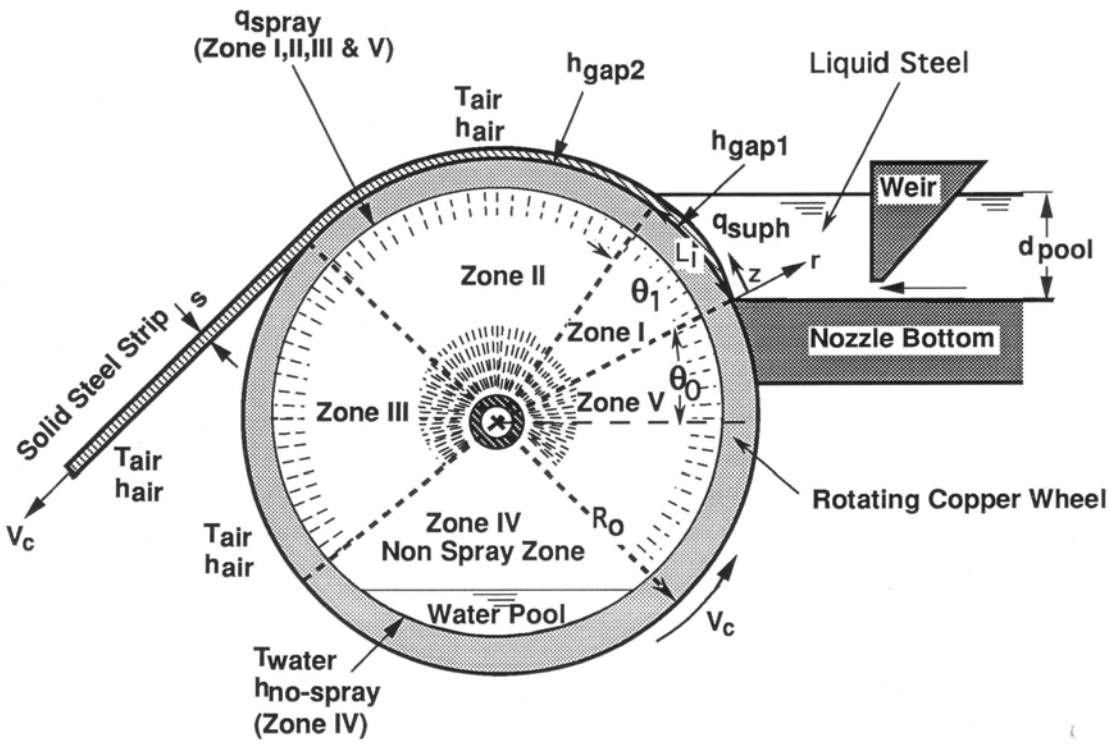

Figure 1(a) Schematic of Single-wheel Thin Strip Casting Process

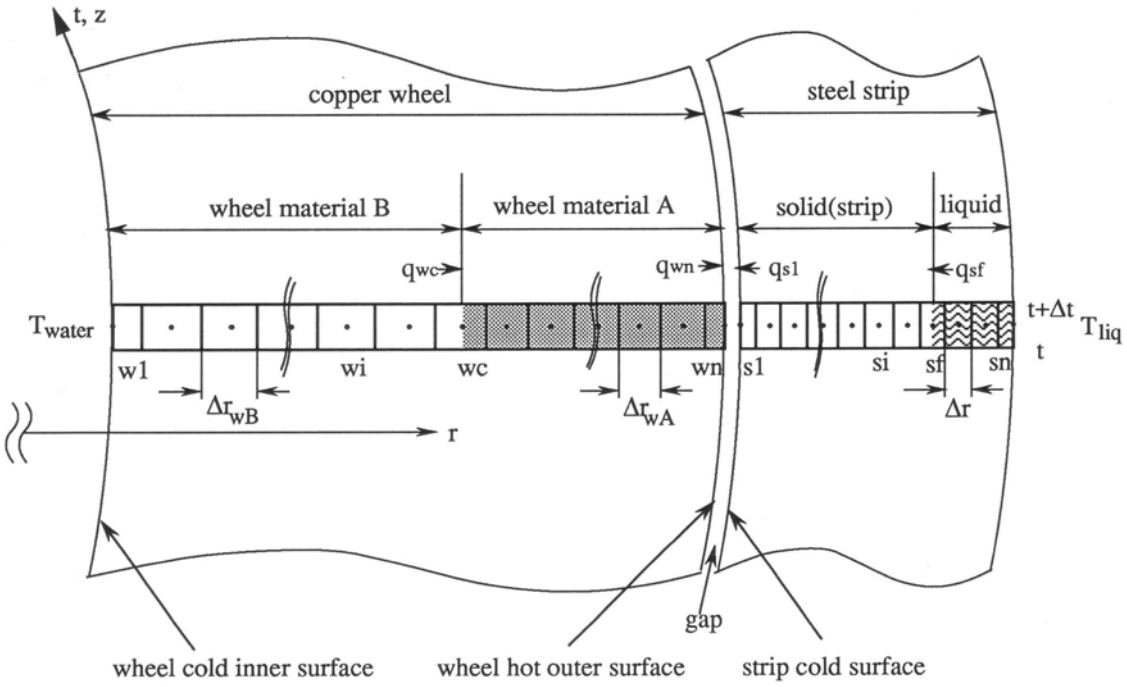

Figure 1 (b) Simulation Domain and Boundary Conditions

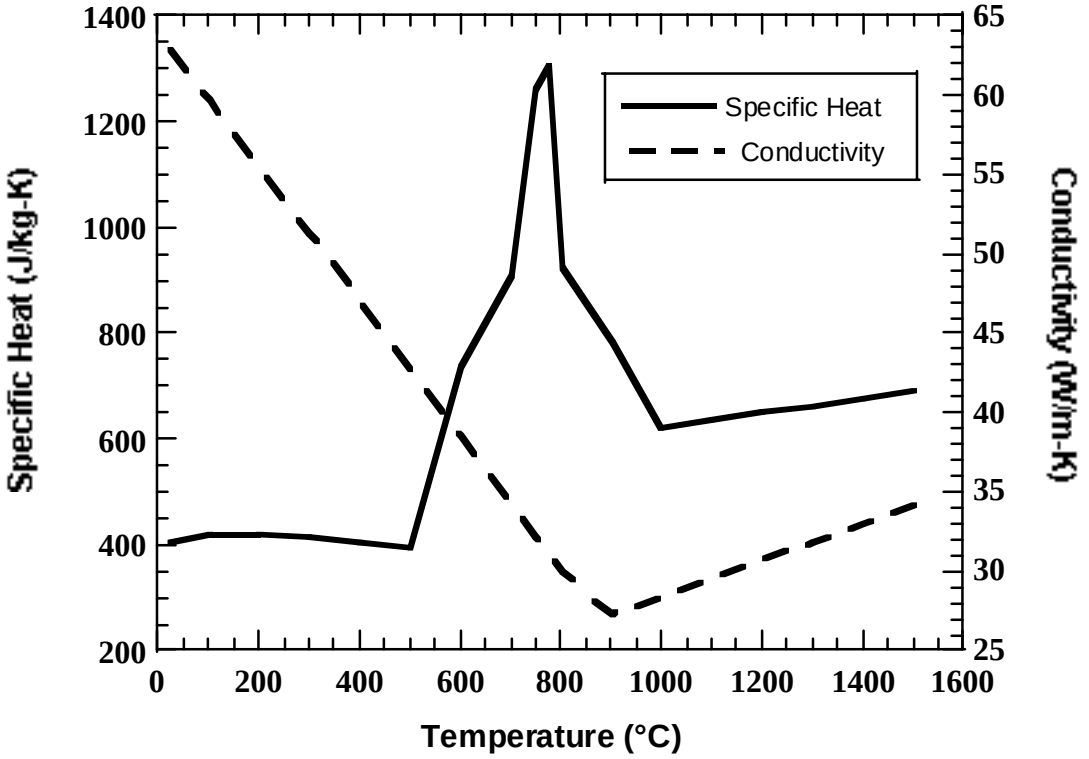

Figure 2 Temperature Dependent Properties Assumed for Plain Carbon Steel

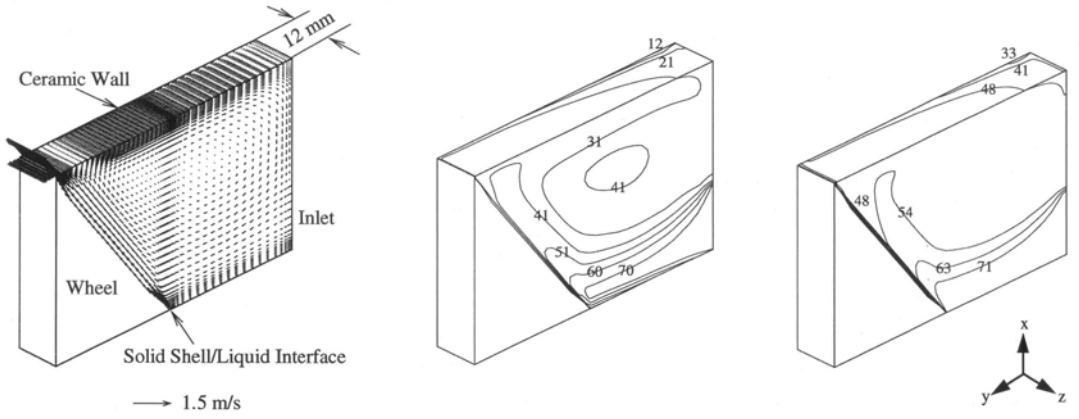

(a) Velocity Field (b) Superheat Temperature Field (10 s) (c) Superheat Temperature Field (Steady State)

Figure 3 Velocity and Superheat Temperature in the Liquid Pool.

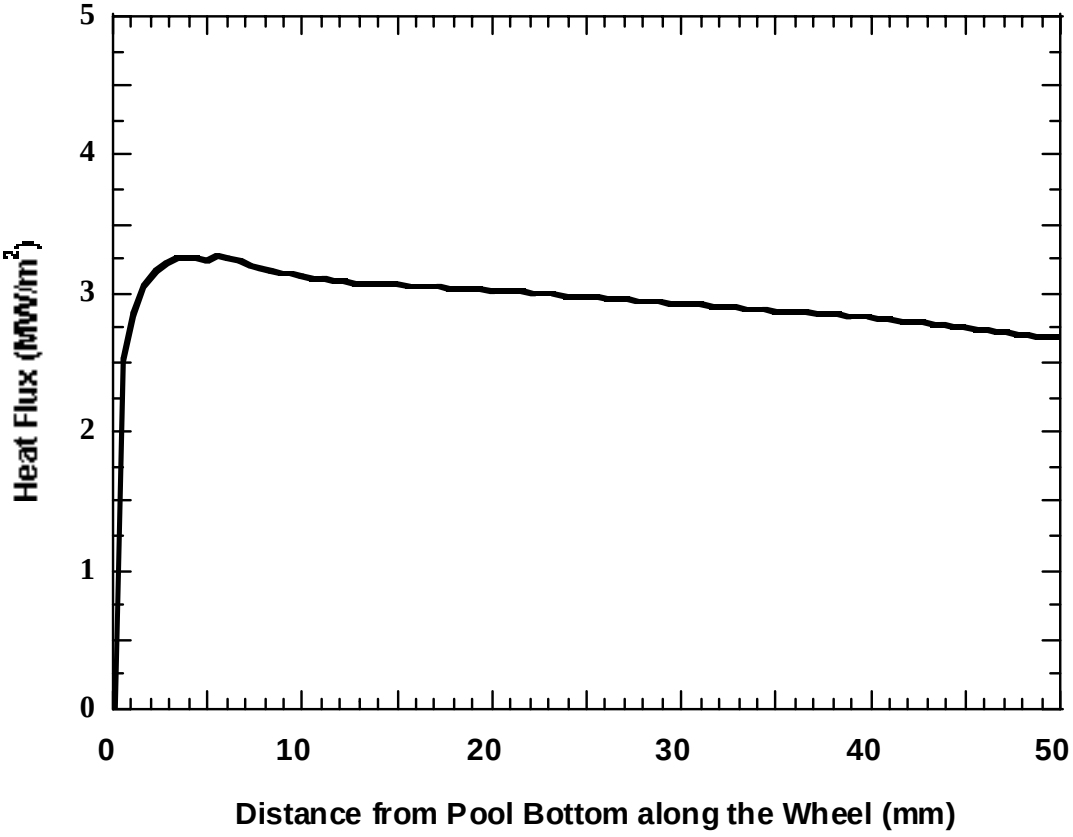

Figure 4 Predicted Superheat Flux to Shell[21]
(V_c = 1.5 m/s, Superheat ýT = 75 ℃)

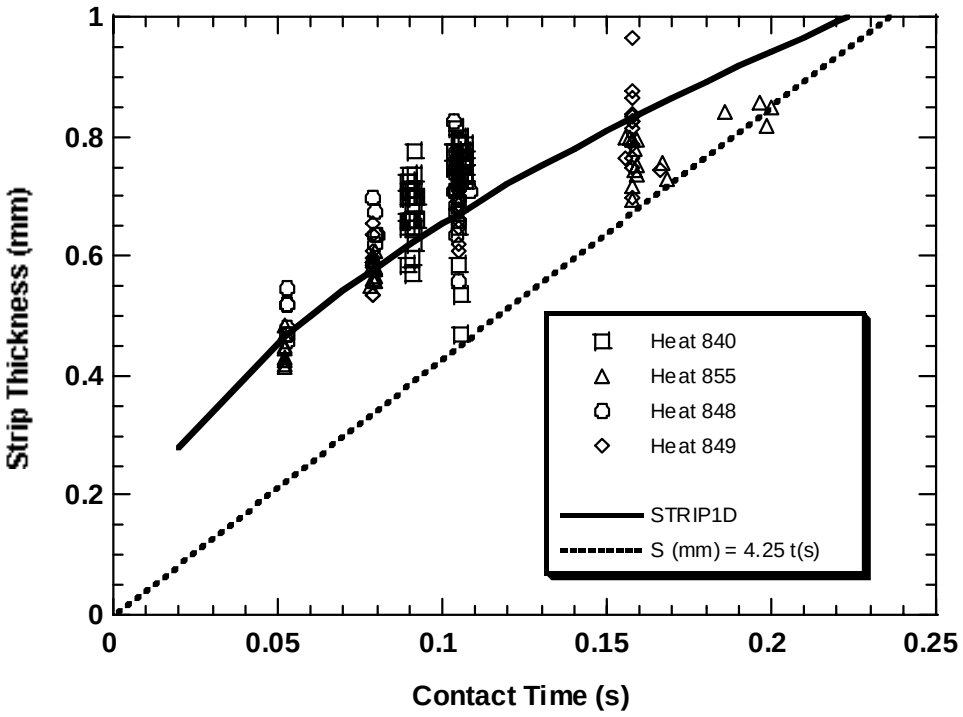

Figure 5 Effect of Contact Time on Final Strip Thicknesses Calculated by STRIP1D, Compared with ARMCO Experimental Data [29] Used for Calibration

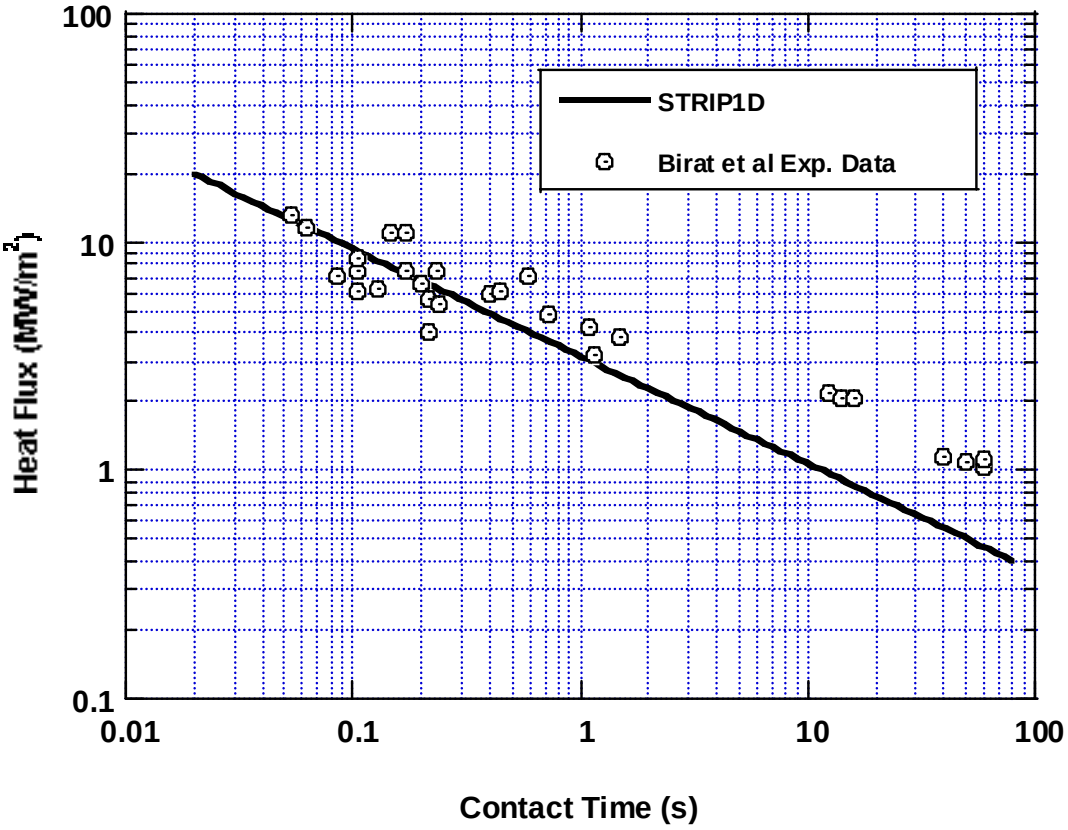

Figure 6 Effect of Contact Time on Heat Flux

(STRIP1D Compared with Experimental Data from Birat et al[4])

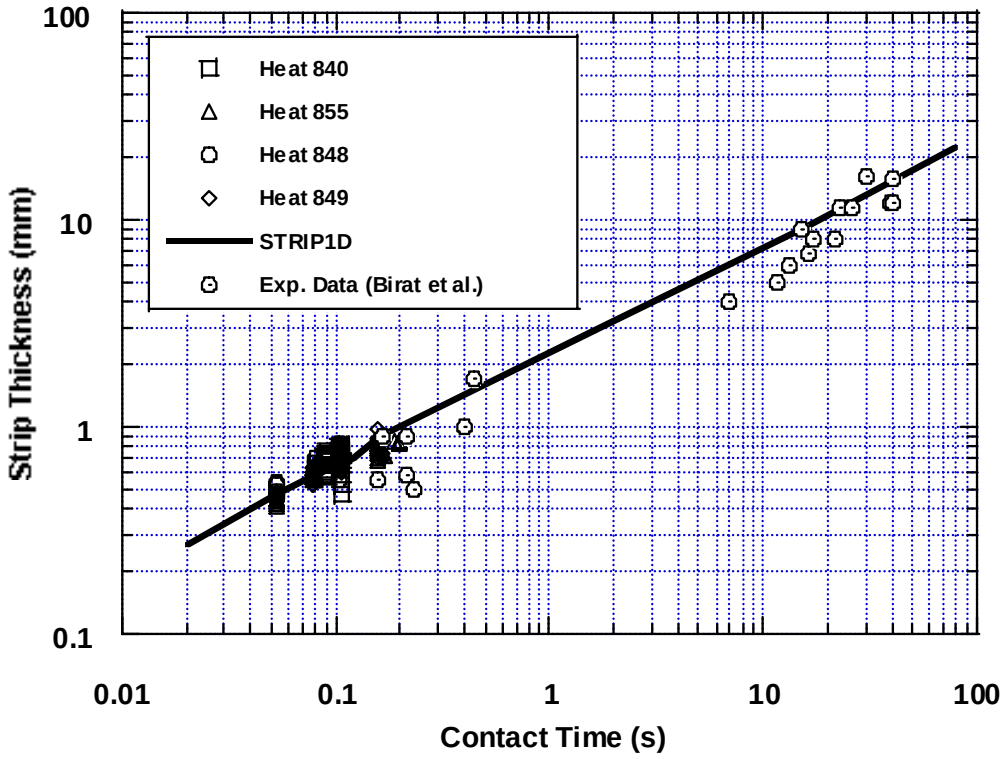

Figure 7 Comparison of STRIP1D Predicted Strip Thickness with Experimental Data (from ARMCO[29] and Birat et al[4])

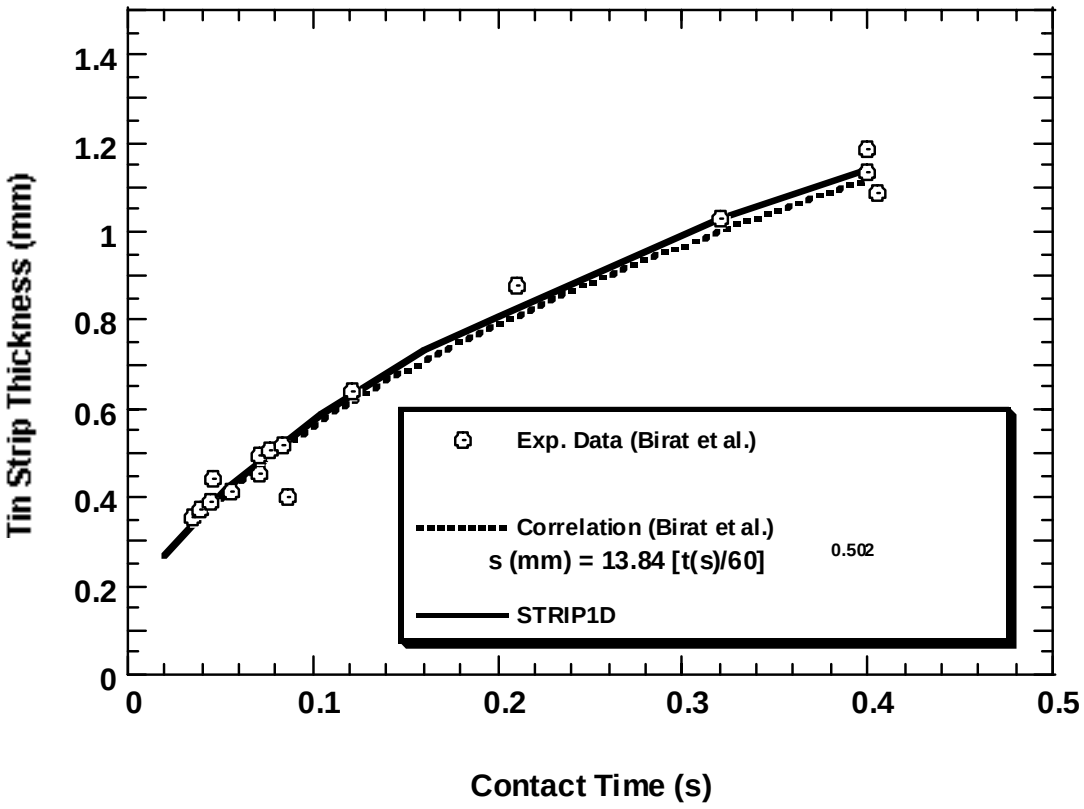

Figure 8 Comparison between Predicted and Measured Strip Thickness for Tin Casting Process[3]

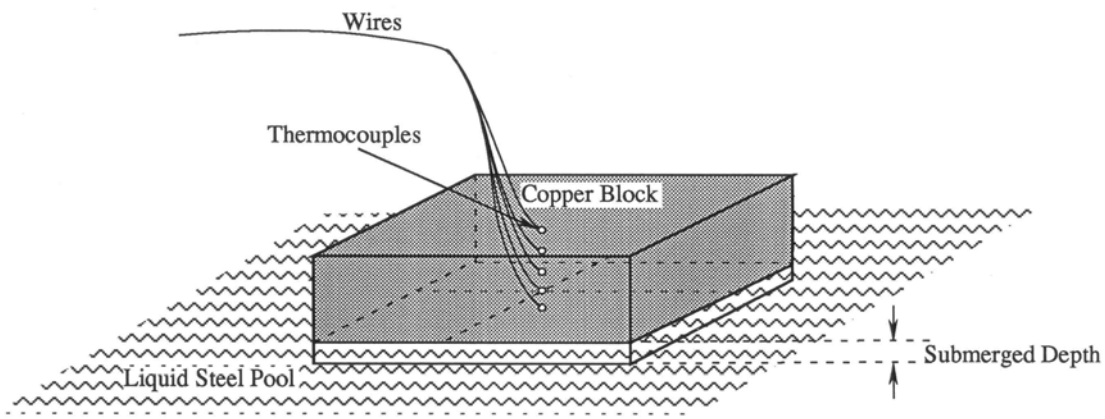

Figure 9 Schematic of Hot-Dip Experimental Set-up

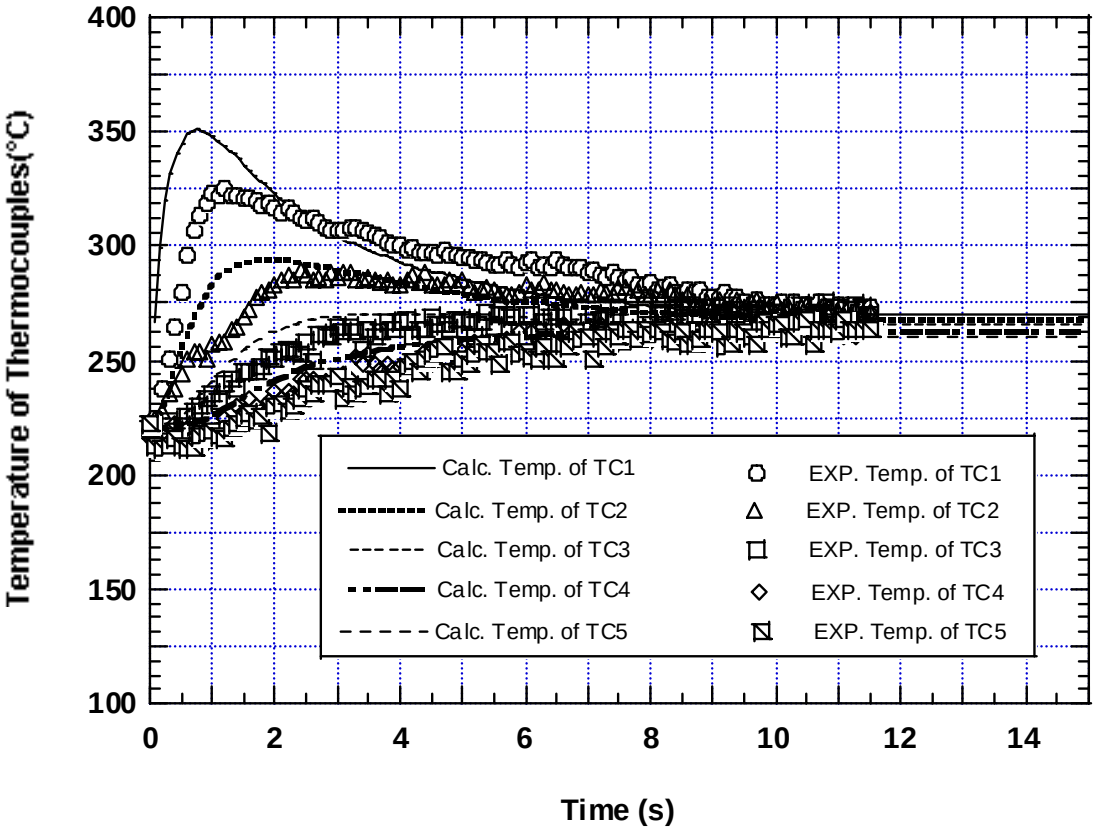

Figure 10 Comparison between Predicted and Measured Thermocouple Temperatures for Dip Experiment [31]

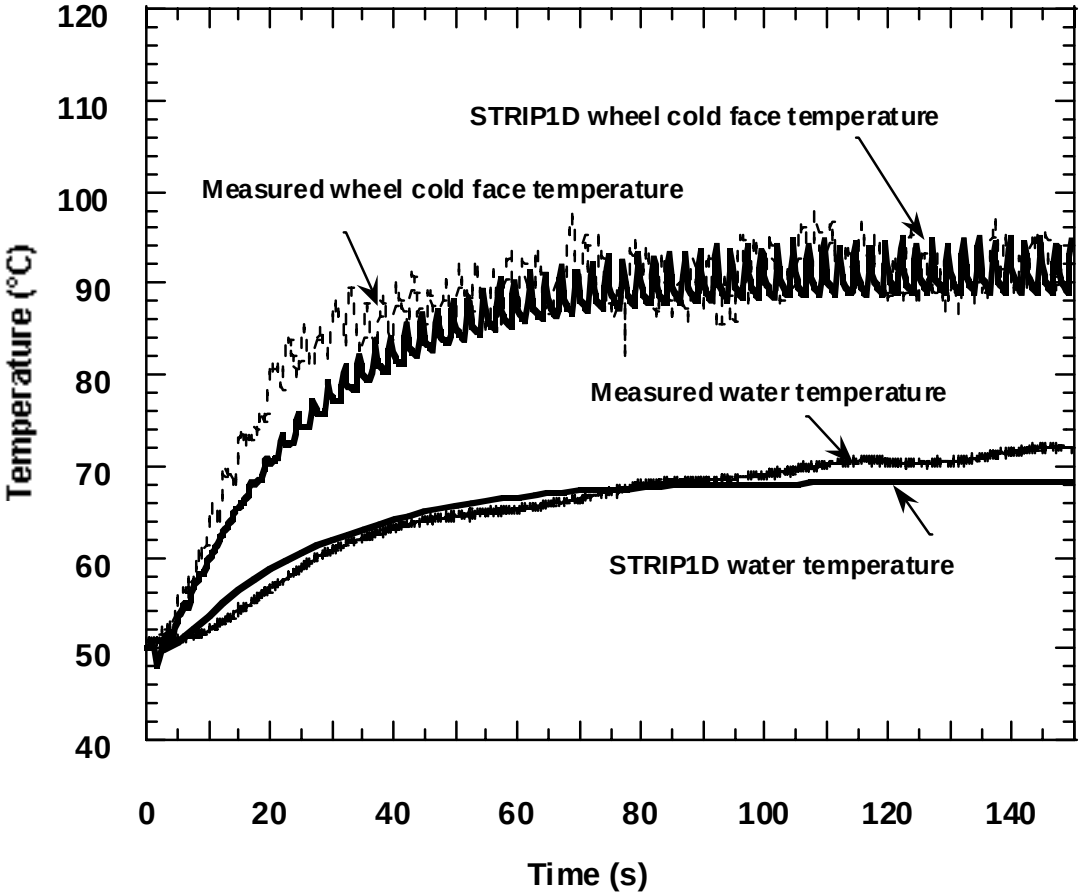

Figure 11 Wheel Cold Face Temperature and Water Temperature Histories (Standard Conditions)

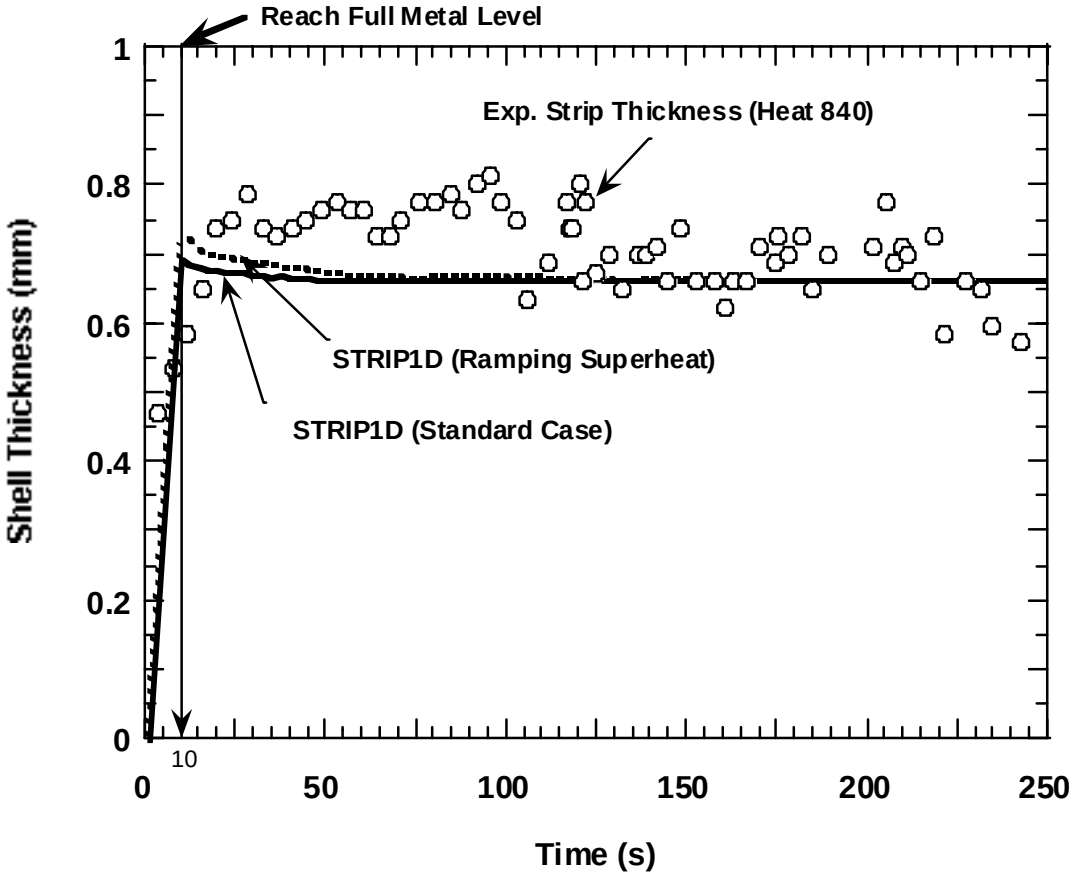

Figure 12 Comparison between Predicted and Measured Final Strip Thickness (Standard Case Versus Ramping Superheat Case)

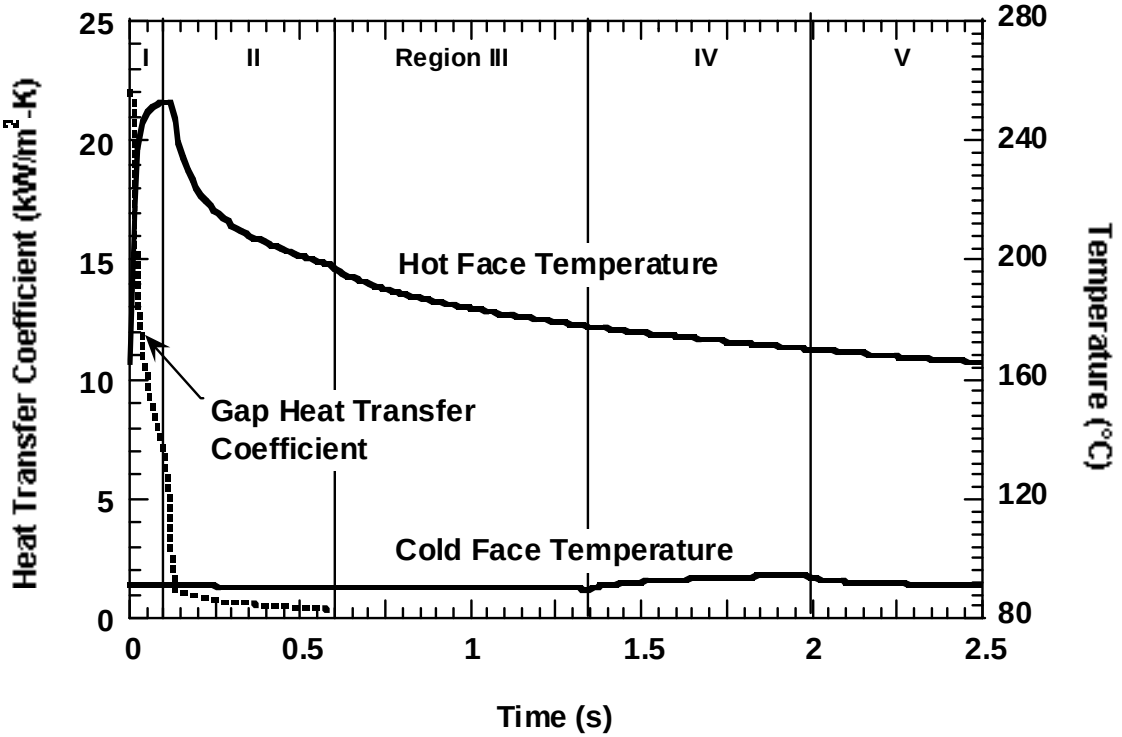

Figure 13 Predicted Wheel Temperature and Gap Heat Transfer Coefficient at Steady State (Standard Conditions)

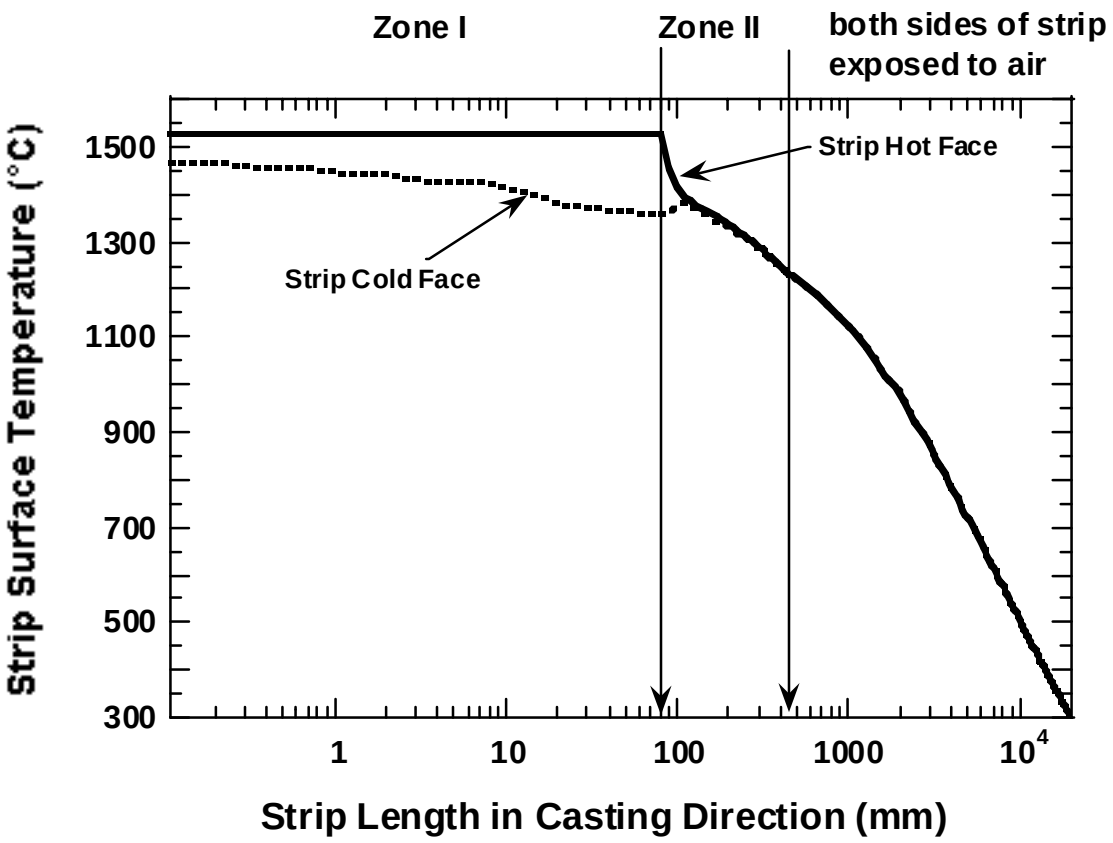

Figure 14 Steady State Strip Hot and Cold Face Temperature
(Standard Conditions)

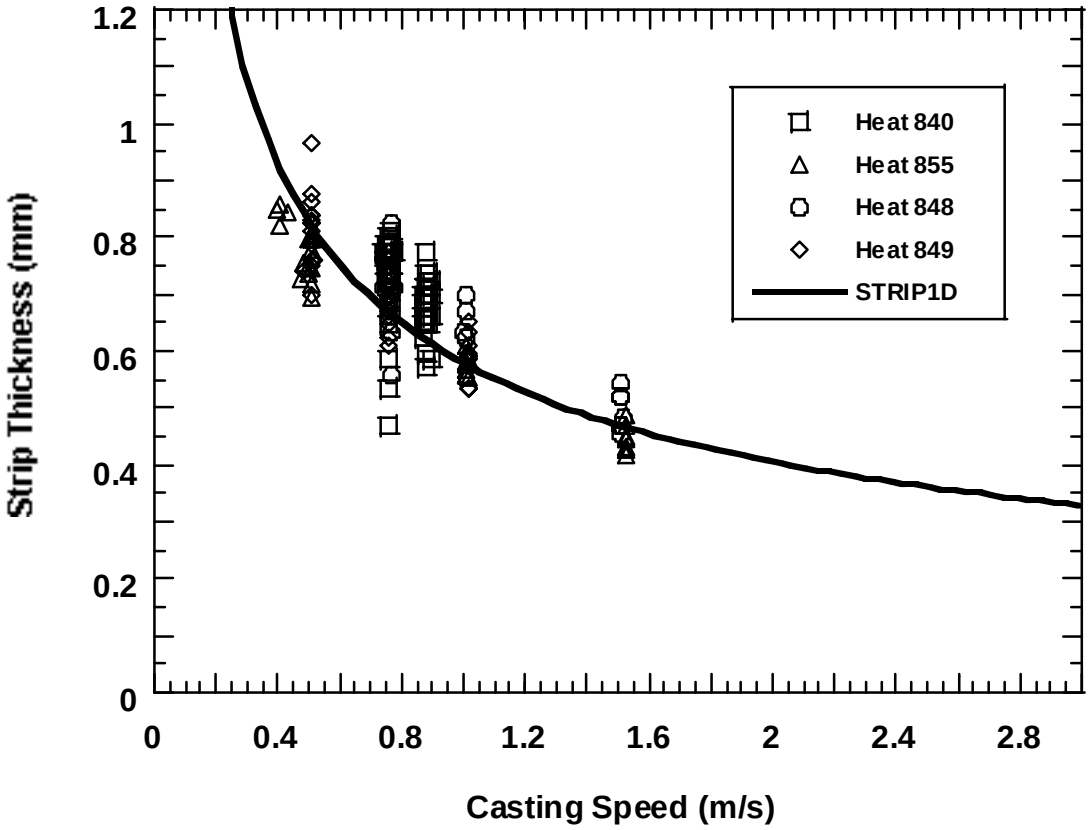

Figure 15 Effect of Casting Speed on Predicted and Measured[29] Final Strip Thickness

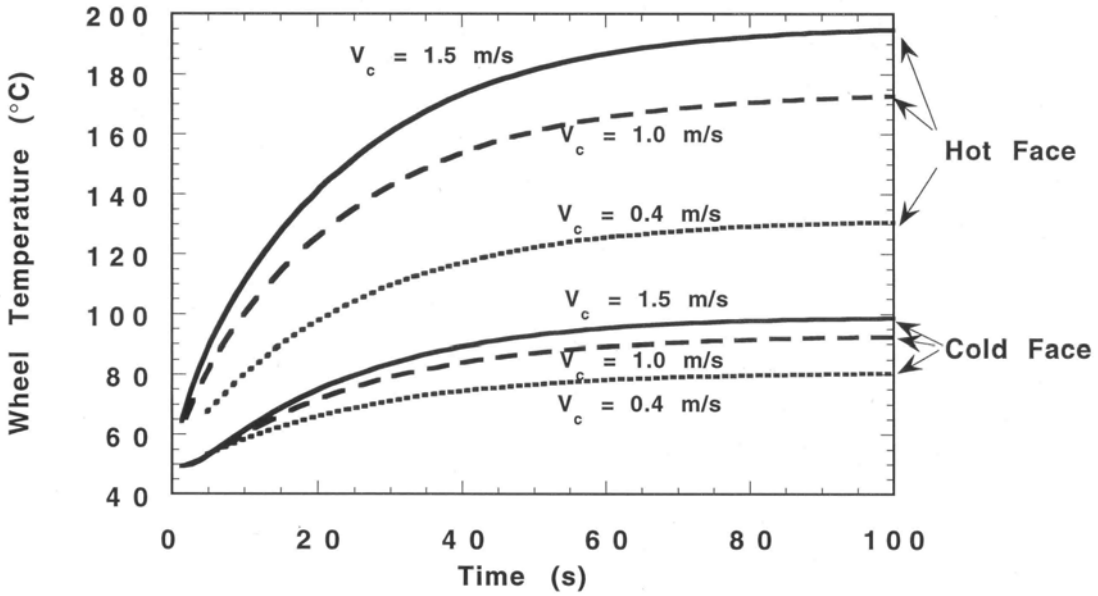

Figure 16 Effect of Casting Speed on Predicted Wheel Temperature on Cold and Hot Faces at z=0

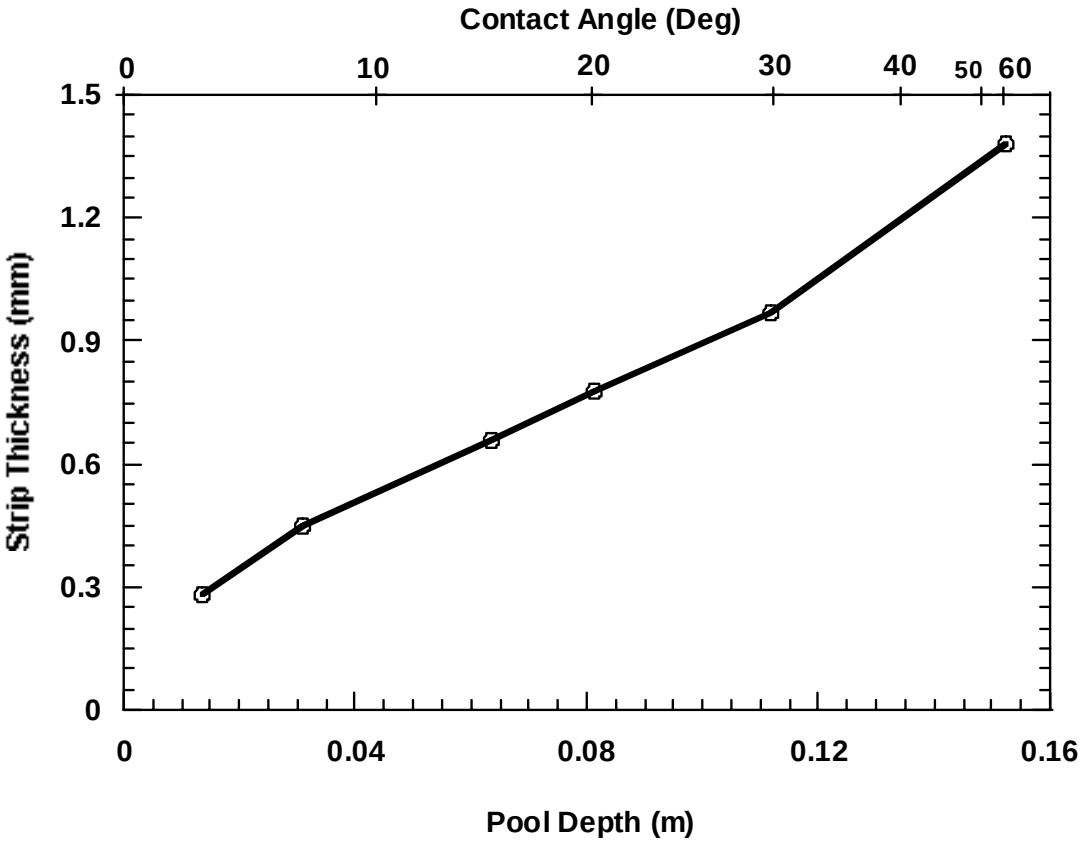

Figure 17 Effect of Pool Depth on Strip Thickness (Standard Conditions)

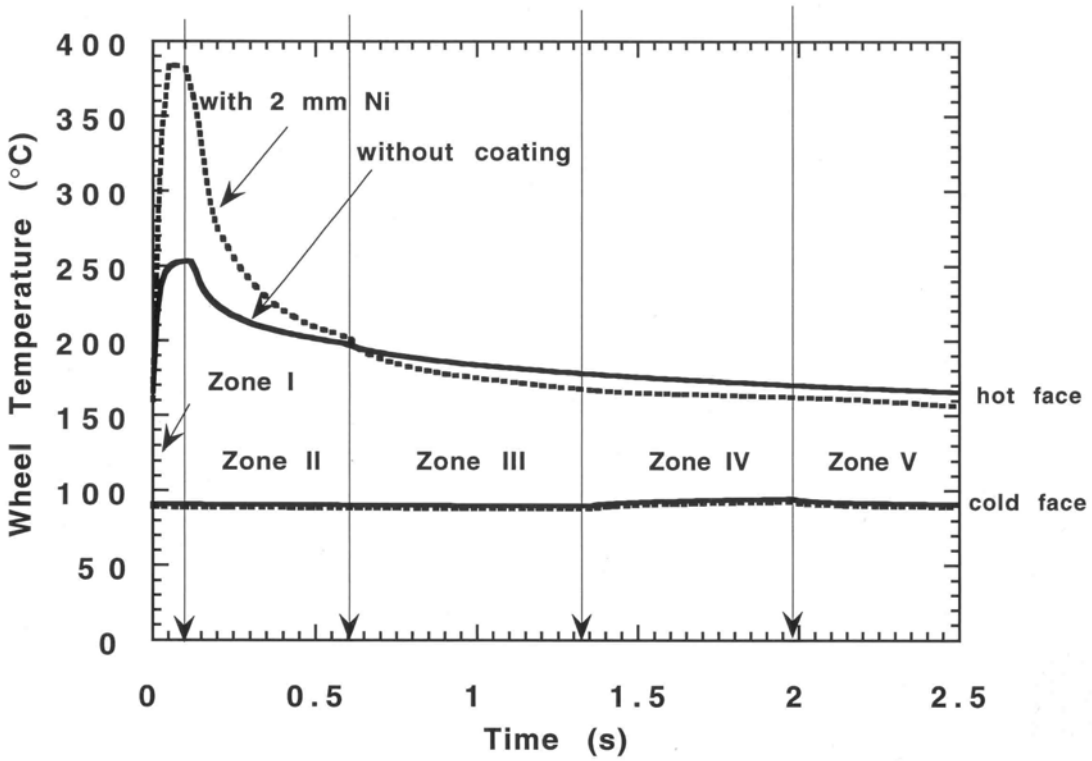

Figure 18 Effect of Wheel Coatings on Steady State Wheel Hot and Cold Face Temperature

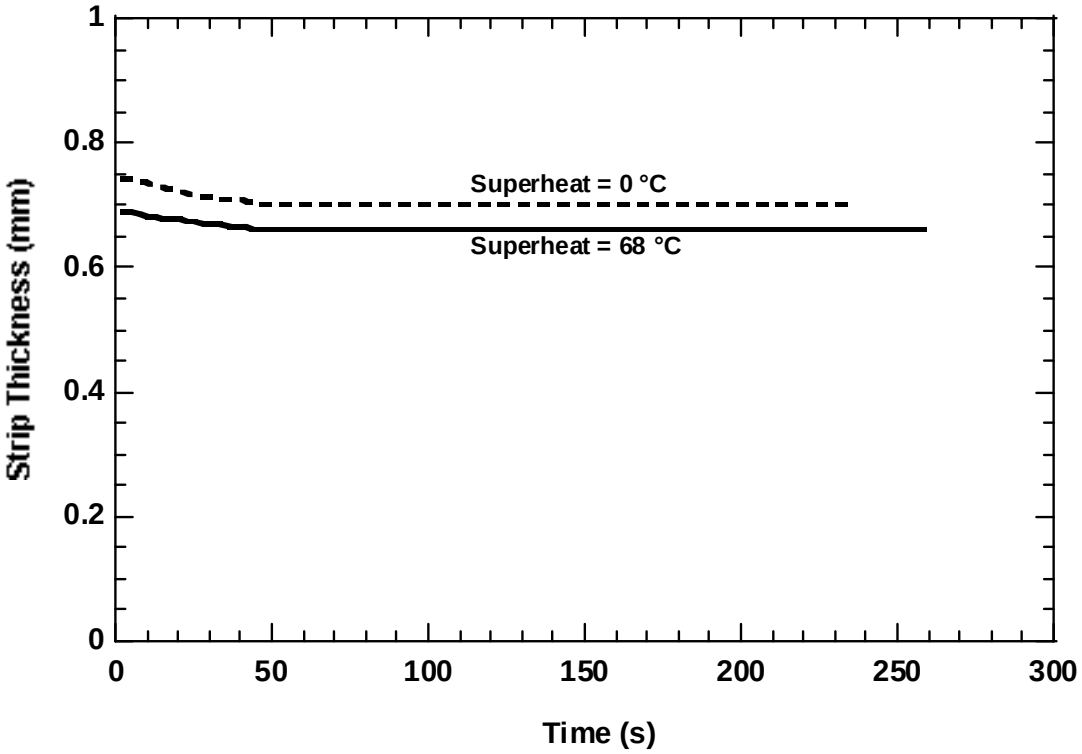

Figure 19 Effect of Superheat on Strip Thickness (Standard Conditions)